NASA/TM–2017-104606/Vol. 47

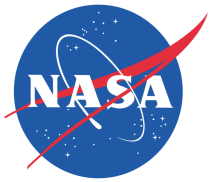

Technical Report Series on Global Modeling and Data Assimilation, Volume 47

Randal D. Koster, Editor

An Evaluation of Teleconnections Over the United States in an Ensemble of AMIP Simulations with the MERRA-2 Configuration of the GEOS Atmospheric Model

Allison B. Marquardt Collow, Sarith P. Mahanama, Michael G. Bosilovich, Randal D. Koster, and Siegfried D. Schubert

National Aeronautics and
Space Administration

Goddard Space Flight Center
Greenbelt, Maryland 20771

May 2017

NASA STI Program ... in Profile

Since its founding, NASA has been dedicated to the advancement of aeronautics and space science. The NASA scientific and technical information (STI) program plays a key part in helping NASA maintain this important role.

The NASA STI program operates under the auspices of the Agency Chief Information Officer. It collects, organizes, provides for archiving, and disseminates NASA's STI. The NASA STI program provides access to the NASA Aeronautics and Space Database and its public interface, the NASA Technical Report Server, thus providing one of the largest collections of aeronautical and space science STI in the world. Results are published in both non-NASA channels and by NASA in the NASA STI Report Series, which includes the following report types:

- TECHNICAL PUBLICATION. Reports of completed research or a major significant phase of research that present the results of NASA Programs and include extensive data or theoretical analysis. Includes compilations of significant scientific and technical data and information deemed to be of continuing reference value. NASA counterpart of peer-reviewed formal professional papers but has less stringent limitations on manuscript length and extent of graphic presentations.
- TECHNICAL MEMORANDUM. Scientific and technical findings that are preliminary or of specialized interest, e.g., quick release reports, working papers, and bibliographies that contain minimal annotation. Does not contain extensive analysis.
- CONTRACTOR REPORT. Scientific and technical findings by NASA-sponsored contractors and grantees.
- CONFERENCE PUBLICATION. Collected papers from scientific and technical conferences, symposia, seminars, or other meetings sponsored or co-sponsored by NASA.
- SPECIAL PUBLICATION. Scientific, technical, or historical information from NASA programs, projects, and missions, often concerned with subjects having substantial public interest.
- TECHNICAL TRANSLATION. English-language translations of foreign scientific and technical material pertinent to NASA's mission.

Specialized services also include organizing and publishing research results, distributing specialized research announcements and feeds, providing help desk and personal search support, and enabling data exchange services. For more information about the NASA STI program, see the following:

- Access the NASA STI program home page at http://www.sti.nasa.gov
- E-mail your question via the Internet to help@sti.nasa.gov
- Fax your question to the NASA STI Help Desk at 443-757-5803
- Phone the NASA STI Help Desk at 443-757-5802
- Write to:

  NASA STI Help Desk
  NASA Center for AeroSpace Information
  7115 Standard Drive
  Hanover, MD 21076-1320

NASA/TM-2017-104606/Vol. 47

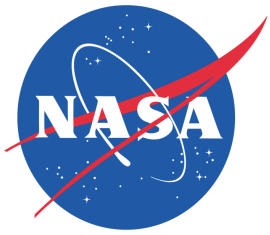

Technical Report Series on Global Modeling and Data Assimilation, Volume 47

Randal D. Koster, Editor

An Evaluation of Teleconnections Over the United States in an Ensemble of AMIP Simulations with the MERRA-2 Configuration of the GEOS Atmospheric Model

Allison B. Marquardt Collow
Universities Space Research Association, Columbia, MD

Sarith P. Mahanama
Science Systems Applications Inc., Lanham, MD

Michael G. Bosilovich
Goddard Space Flight Center, Greenbelt, MD

Randal D. Koster
Goddard Space Flight Center, Greenbelt, MD

Siegfried D. Schubert
Science Systems Applications Inc., Lanham, MD

National Aeronautics and
Space Administration

Goddard Space Flight Center
Greenbelt, Maryland 20771

May 2017

Level of Review: This material has been technically reviewed by technical management

Available from

NASA STI Program
Mail Stop 148'
NASA Langley Research Center
Hampton, VA 23681–2199

National Technical Information Service
5285 Port Royal Road
Springfield, VA 22161
703–605–6000

This document is available for downloaded from the NASA Technical Reports Server (NTRS).
https://ntrs.nasa.gov

Abstract

The atmospheric general circulation model that is used in NASA's Modern Era Retrospective Analysis for Research and Applications – Version 2 (MERRA-2) is evaluated with respect to the relationship between large-scale teleconnection patterns and daily temperature and precipitation over the United States (US) using a ten-member ensemble of simulations, referred to as M2AMIP. A focus is placed on four teleconnection patterns that are known to influence weather and climate in the US: El Niño Southern Oscillation, the Pacific Decadal Oscillation, the North Atlantic Oscillation, and the Pacific-North American Pattern. The monthly and seasonal indices associated with the patterns are correlated with daily temperature and precipitation statistics including: (i) monthly mean 2 m temperature and precipitation, (ii) the frequency of extreme temperature events at the 90^{th}, 95^{th}, and 99^{th} percentiles, and (iii) the frequency and intensity of extreme precipitation events classified at the 90^{th}, 95^{th}, and 99^{th} percentiles. Correlations obtained with M2AMIP data – and thus the strength of teleconnections in the free-running model – are evaluated through comparison against corresponding correlations computed from observations and from MERRA-2. Overall, the strongest teleconnections in all datasets occur during the winter and coincide with the largest agreement between the observations, MERRA-2, and M2AMIP. When M2AMIP does capture the correlation seen in observations, there is a tendency for the spatial extent to be exaggerated. The weakest agreement between the data sources, for all teleconnection patterns, is in the correlation with extreme precipitation; however there are discrepancies between the datasets in the number of days with at least 1 mm of precipitation: M2AMIP has too few days with precipitation in the Northwest and the Northern Great Plains and too many days in the Northeast. In JJA, M2AMIP has too few days with precipitation in the western two-thirds of the country and too many days with precipitation along the east coast.

Table of Contents

1. Introduction

Teleconnection patterns, typically comprised of two to four centers of action of low frequency variability that are, at times, 2500-6000 km apart (Barnston and Livezey, 1987), can persist on timescales of weeks to months but impact day-to-day weather around the globe by influencing the planetary-scale circulation, including the atmospheric jet streams (Wallace and Gutzler, 1981). The study of teleconnections dates back to the early 1900's when Sir Gilbert Walker sought to create long-term forecasts of the Indian monsoon; using a correlation analysis, he noted a connection between a swaying of atmospheric pressure in the Pacific and Indian Oceans and world weather (Katz, 2002). This theory is now a well-known and documented atmospheric teleconnection associated with the El Niño/Southern Oscillation (ENSO) (eg. Bjerknes, 1969; Lim and Kim, 2007; Zhang et al., 2011). Robust teleconnection patterns, such as the atmospheric patterns related to ENSO, form the basis of seasonal climate predictions (Goddard et al., 2001) and have been documented in countless journal articles. Due to the importance of teleconnections, this document serves as an evaluation of the accuracy of the simulated teleconnections over the US in version 5.12.4 of the Goddard Earth Observing System (GEOS-5) atmospheric model, which was used to produce the Modern Era Retrospective Analysis for Research and Applications – Version 2 (MERRA-2).

ENSO is perhaps the most well-known large-scale teleconnection pattern and is often in the media regarding its impact on the United States. A recent focus has been on the potential role of El Niño in alleviating drought on the US West Coast, with some unexpected outcomes (e.g., the strong El Nino during 2015/16 that did not produce the expected increased rainfall in southern California) highlighting the complicated relationship between ENSO and precipitation in California (e.g., Seager et al. 2015; Hoell et al., 2016). The cool phase of ENSO, La Niña, has been connected to droughts in the Southern Great Plains (e.g., Ting et al. 1997; Schubert et al. 2009; Hoell et al., 2014). Another ocean-induced atmospheric teleconnection that impacts the United States is the Pacific Decadal Oscillation (PDO; Mantua et al. 1997; Zhang et al, 1997), which is determined by sea surface temperatures (SSTs) north of 20° latitude in the Pacific Ocean. During the positive phase of the PDO, the tendency over the US is for below-normal temperatures along the east coast, above-average temperatures in the Northwest, above-normal precipitation in the Southwest, and below-normal precipitation in the East (e.g., Mantua and Hare 2002; McAfee, 2014).

Not all teleconnections are connected to sea surface temperatures. The North Atlantic Oscillation (NAO) and Pacific-North American Pattern (PNA) are modes of climate variability that are generally believed to be internal to the atmosphere with intrinsic times scales less than two weeks (e.g., Feldstein 2002; Schubert and Lim 2013), though they have impacts on monthly and longer time scales and, as discussed later in the text (sections 3.3 and 3,4; see also Straus and Shukla 2002; Mosedale et al. 2006), appear to be modulated by SST. The NAO primarily impacts the weather in Europe and storm tracks in the North Atlantic but has also been

documented to influence the temperature in the eastern United States (e.g., Hurrell et al., 1997). On the other hand, the PNA has strong ties to the jet stream over the United States, influencing the temperature and precipitation patterns across the entire country (e.g., Leathers et al., 1991).

The strengths of the teleconnections between these four teleconnection patterns and continental precipitation and 2m air temperature in the US are evaluated here in the observations, in MERRA-2, and in a ten-member ensemble of simulations with the free-running atmospheric general circulation model, the same model that was used in producing MERRA-2. In so doing, we evaluate the realism of the teleconnections in the free-running model, teleconnections that are fundamental to the success of subseasonal-to-seasonal forecasts produced with the model. In addition to the connections to mean precipitation and temperature, we consider here daily extreme temperature and precipitation events.

2. Datasets and Methodology

2.1 MERRA-2

MERRA-2 is a reanalysis product that assimilates global conventional and satellite observations to create a gridded, temporally and spatially consistent view of weather and climate extending from January 1980 through near real time (Gelaro et al., 2017). Using version 5.12.4 of the Goddard Earth Observing System (GEOS-5), MERRA-2 output data have a temporal resolution of one hour and a spatial resolution of 0.5° latitude by 0.625° longitude, with 72 vertical levels (Bosilovich et al., 2015). Improvements were made to the physical parameterizations compared to MERRA; a description of these changes can be found in Molod et al. (2015). Additional updates include a global mass balance (Takacs et al., 2016), observations-corrected precipitation forcing for the land (Reichle et al., 2017), and the introduction of interactive and assimilated aerosols (Randles et al., 2017).

Boundary conditions for SST and sea ice concentration (SIC) stem from three distinct datasets as there is no reliable, high resolution, continuous data product available extending back to 1980. Prior to January 1982, monthly 1° boundary conditions as described by Taylor et al. (2000) are used. This dataset provides the boundary conditions for the Atmospheric Model Intercomparison Project (AMIP). Between 1982 and 2006, daily, 1/4° SST and SIC from Reynolds et al. (2007) are used. After April 2006, the Operational Sea Surface Temperature and Sea Ice Analysis (OSTIA) system is used, with a temporal resolution of one day and a spatial resolution of 1/20° (Donlon et al., 2012). All three datasets are interpolated to a 1/4° grid; however, there is no merging of climatologies between the datasets. Additional details regarding SST and SIC can be found in section 8 of Bosilovich et al. (2015).

Details regarding assimilated observations can be found in McCarty et al. (2016), and an extensive evaluation of MERRA-2 can be found in Bosilovich et al. (2015). Daily statistics of temperature, including daily mean, maximum, and minimum, are from the statD_2d_slv file

collection (GMAO, 2015a), while daily statistics of precipitation are computed from hourly data in the tavg1_2d_flx file collection (GMAO, 2015b). The 500hPa heights presented in section 3 are from the monthly-averaged data in the tavgM_2d_slv file collection (GMAO, 2015c).

The MERRA-2 dataset includes two variables for total precipitation, PRECTOT and PRECTOTCORR. PRECTOT is model-generated through application of the Relaxed Arakawa-Schubert convective scheme followed by the prognostic large-scale cloud condensate scheme, PrognoCloud (Rienecker et al., 2008). This is the precipitation that is used to compute the correlations shown in section 3. PRECTOTCORR is an observations-corrected version of the model-generated precipitation that is used to force the land surface and for the wet deposition of aerosols (Riechle et al., 2017). The observations-corrected precipitation merges the model-generated precipitation (PRECTOT) with the CPC Unified Gauge-Based Analysis of Global Daily Precipitation (CPCU) product and the CPC Merged Analysis of Precipitation (CMAP) product. Although PRECTOTCORR is not included in our analysis, it can influence our results for MERRA-2 as land surface properties such as soil moisture contribute to the energy and water fluxes seen by the atmosphere. More information on the observations-corrected precipitation can be found in Riechle et al. (2017).

2.2 M2AMIP

The ten AMIP-style simulations with the atmospheric model used in MERRA-2 cover the time period of January 1980 through December 2015. This ensemble of simulations is referred to here as M2AMIP; note that AMIP stands for Atmospheric Model Intercomparison Project, a project that outlines a common simulation protocol (Gates, 1992). The M2AMIP simulations were performed in an identical manner to MERRA-2 (e.g., employing the same SST data, GHGs, resolution, etc.) except, of course, that they did not assimilate observations and did not use observations-corrected precipitation to drive the land surface. Initial conditions for each M2AMIP ensemble member were taken from different days of November 1979 during the MERRA-2 spin up period. In assessing the veracity of the model teleconnections, each ensemble member is considered individually (as opposed to analyzing the ensemble mean time series) to allow a proper comparison with the relationships derived from the observations or MERRA-2, neither of which can take advantage of ensemble averaging. The relationships (e.g., correlations) computed from individual ensemble members are averaged over the 10 ensemble members to give a final model estimate. Given this final averaging, the model-derived relationships are statistically more robust than those estimated from the observations or MERRA-2.

2.3 Observations

Precipitation observations come from the Climate Prediction Center's (CPC) Unified Gauge-Based Analysis of Daily Precipitation (Chen and Xie, 2008). This is a gridded product at a 0.25° resolution that is available from January 1948 through the present, spanning the continental United States. The daily values are centered at 0z. Observed precipitation was re-gridded to the spatial resolution of MERRA-2 and M2AMIP prior to analysis. Daily mean, minimum and maximum temperature data at 1,218 stations in the United States were obtained from the Global

Historical Climatology Network (GHCN). This dataset combines numerous sources of observations around the globe as described by Menne et al. (2012). Since this is not a gridded product, correlations are calculated on a station-by-station basis.

2.4 Seasonal Climatology of Temperature and Precipitation

Biases in the seasonal climatology of temperature or precipitation in any of the data sets can influence teleconnection relationships. MERRA-2 was evaluated with regard to the observations by Bosilovich et al. (2015), who showed anomaly correlations of summertime precipitation exceeding 0.9 for 6 out of 8 regions across the continental United States and above 0.8 for the Midwest and Southwest regions. The report also showed agreement between MERRA-2 and observed mean 2 m temperature; it cautions, however, that there is a cool daytime bias that cancels out the warm nighttime bias over land.

A comparison between MERRA-2 and M2AMIP ensemble-average precipitation and 2 m temperature is provided, for each season, in Figures 2.4.1 through 2.4.4. Regardless of season, M2AMIP tends to have a dry bias for most of the country that is most pronounced in the Great Plains during JJA. Exceptions are seen over higher terrain in DJF (Figure 2.4.1e) and on the east coast in JJA (Figure 2.4.3e). Temperature differences between MERRA-2 and M2AMIP are more dependent on season. M2AMIP is cooler than MERRA-2 across most of the country, particularly in the north, during DJF (Figure 2.4.1e). The same pattern in temperature difference is present in MAM; however, the cool bias in M2AMIP weakens and a warm bias is evident in the Southern Great Plains (Figure 2.4.2f). By the summer, the warm bias in M2AMIP spreads across the entire continental United States (Figure 2.4.3f), and it continues through the fall, though weaker (Figure 2.4.4f). Much of the temperature bias in M2AMIP appears to be linked to biases in the radiation at the surface. M2AMIP has less longwave radiation absorbed at the surface during DJF, particularly in the northern part of the country, and it has too much shortwave radiation, by as much as 35 W m^{-2} in the center of the country, reaching the surface during the summer (see online supplemental library). However, the analysis increments, which are used to constrain MERRA-2 to the observations, also play a role in the temperature differences seen between MERRA-2 and M2AMIP.

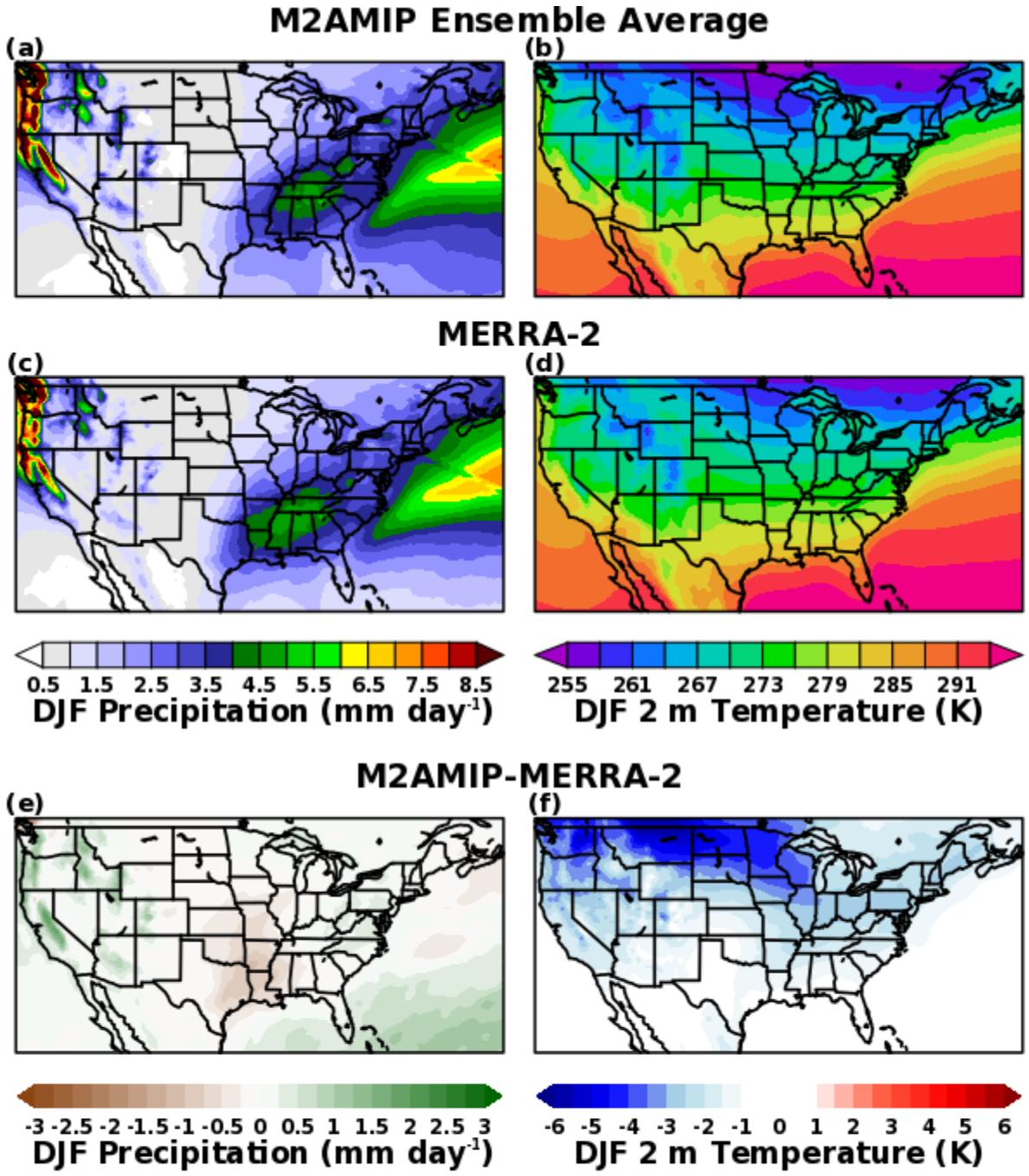

Figure 2.4.1: Mean precipitation and 2 m temperature during DJF in (a, b) M2AMIP, (c, d) MERRA-2, and (e, f) the difference between M2AMIP and MERRA-2 for the period of 1980 through 2015.

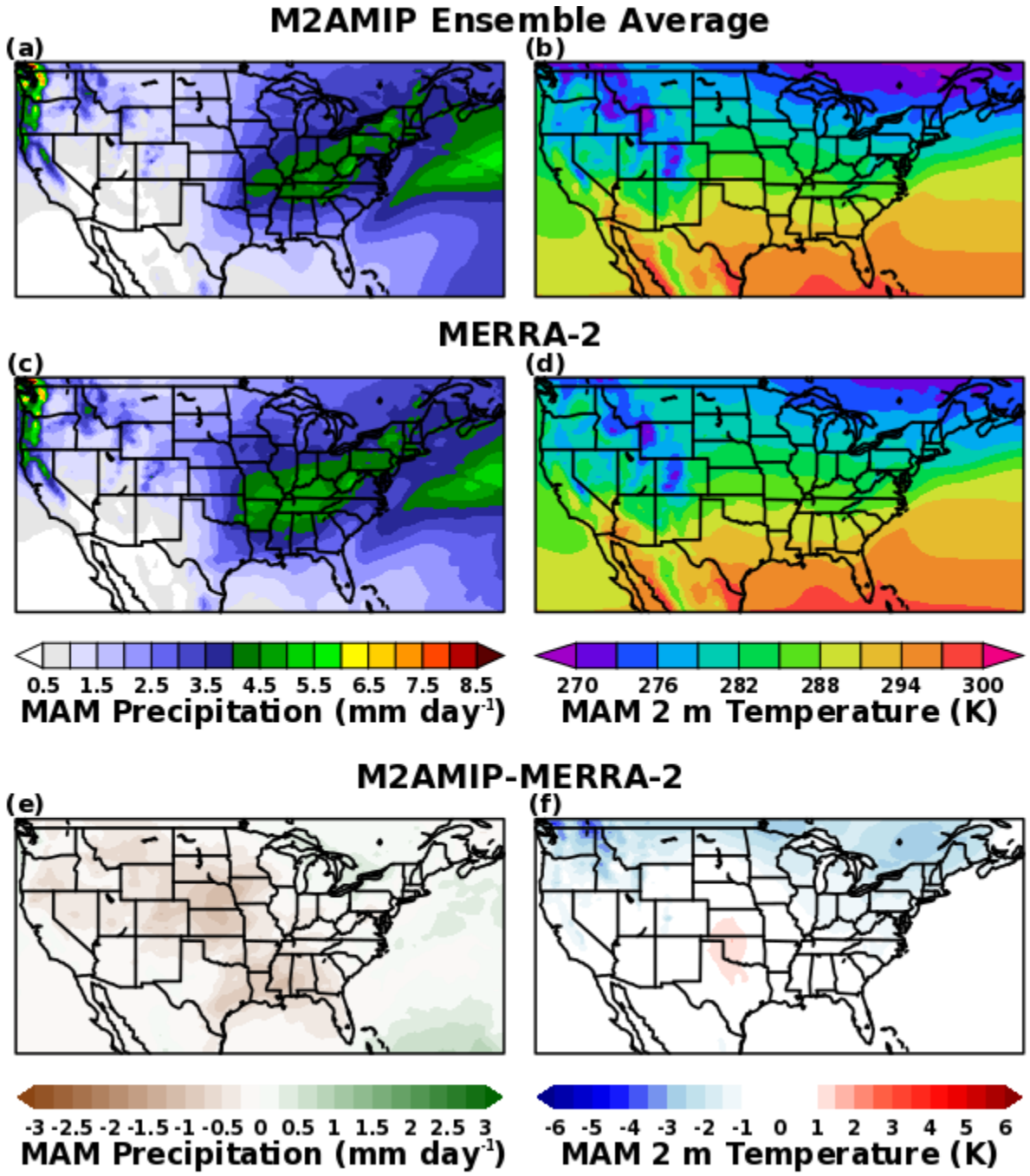

Figure 2.4.2: Mean precipitation and 2 m temperature during MAM in (a, b) M2AMIP, (c, d) MERRA-2, and (e, f) the difference between M2AMIP and MERRA-2 for the period of 1980 through 2015.

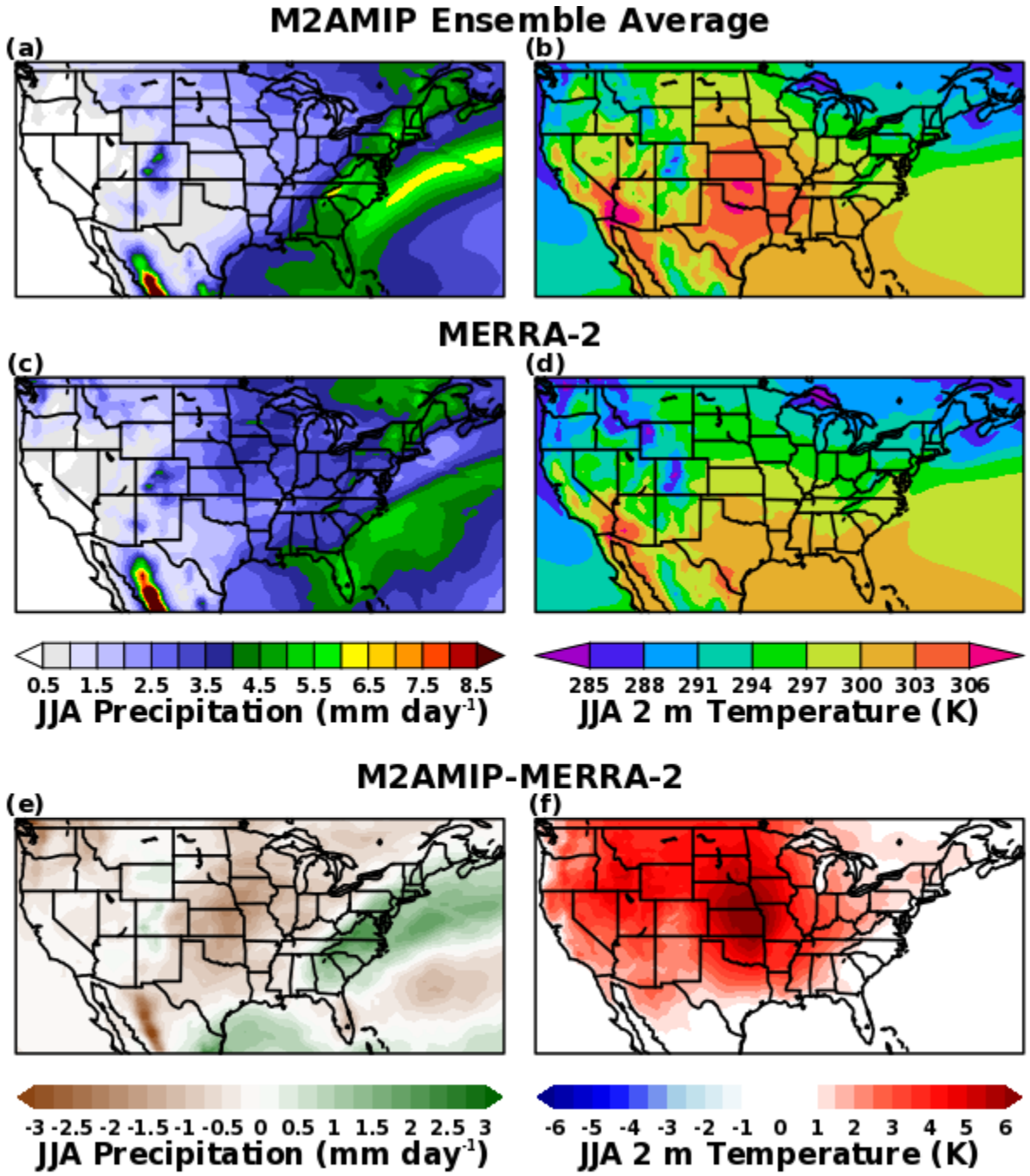

Figure 2.4.3: Mean precipitation and 2 m temperature during JJA in (a, b) M2AMIP, (c, d) MERRA-2, and (e, f) the difference between M2AMIP and MERRA-2 for the period of 1980 through 2015.

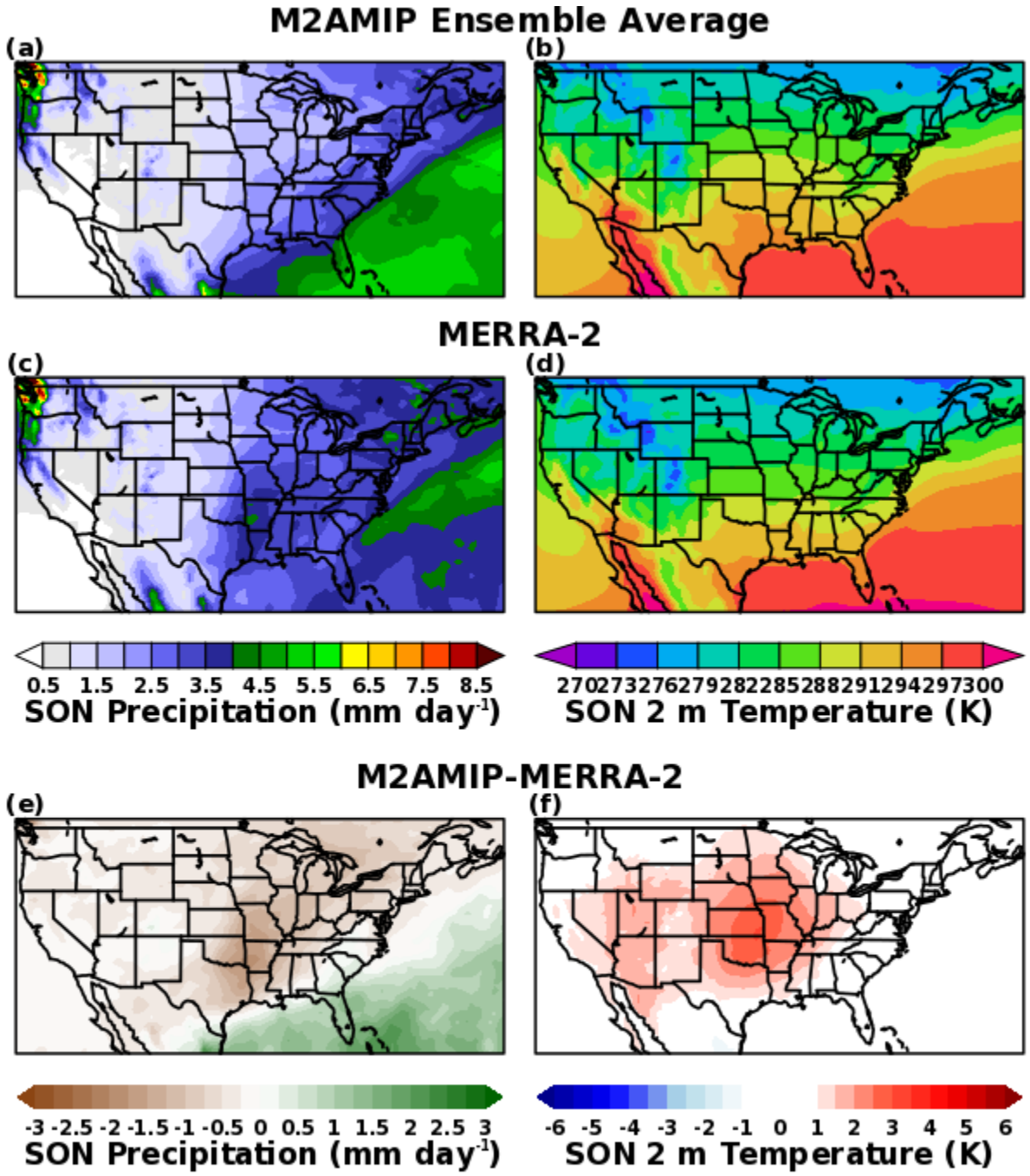

Figure 2.4.4: Mean precipitation and 2 m temperature during SON in (a, b) M2AMIP, (c, d) MERRA-2, and (e, f) the difference between M2AMIP and MERRA-2 for the period of 1980 through 2015.

2.5 Climate Indices

Four well-documented large-scale modes of climate variability were selected for analysis in this study: ENSO, PDO, NAO, and PNA. Monthly values of indices representing these climate features were downloaded from the Physical Science Division of NOAA's Earth Science Research Laboratory; these data can be found at https://www.esrl.noaa.gov/psd/data/climateindices/list/.

ENSO (the El Niño / Southern Oscillation) and the PDO (Pacific Decadal Oscillation) are both indices based on SST anomalies, with ENSO representing the tropical ocean and the PDO representing the northern Pacific Ocean. The average SST anomaly in the Niño3.4 region, located between 5°N, 5°S, 170°W and 120°W, was selected to represent ENSO, as is common in the literature. The PDO is calculated using the leading principal component of monthly sea surface temperature anomalies in the Pacific Ocean north of 20°N (Zhang et al, 1997; Mantua et al., 1997). Seasonal averages for December, January, and February (DJF), March, April, and May (MAM), June, July, and August (JJA), and September, October, and November (SON) of the ENSO and PDO indices are derived from the monthly observational data and are then regressed against precipitation and temperature over the US in the observations, MERRA-2, and M2AMIP. The computed correlation between the large-scale indices and the continental variables is interpreted as a measure of teleconnection strength.

Because atmosphere-based indices tend to vary on shorter time scales than SST-based indices, monthly values for the NAO (North Atlantic Oscillation) and PNA (Pacific/North American pattern) are examined here. To obtain the monthly values for the indices, rotated empirical orthogonal functions (REOFs) were used to isolate the leading atmospheric patterns connected to the NAO and PNA (Barnston and Livezey, 1987). Note that the same time series of NAO and PNA indices are correlated against US precipitation and air temperature from both the observations and MERRA-2, whereas independently computed time series of NAO and PNA indices are computed from the M2AMIP simulations for correlation against the M2AMIP continental variables.

Our analysis of the NAO is constrained to DJF, as this tends to be more of a wintertime phenomenon. The REOF for the NAO used monthly mean sea level pressure within a domain of 20° to 80°N and 90°W to 40°E. Rather than computing the REOF for each ensemble member individually, the REOF calculation was based on data from all M2AMIP ensemble members together. The MERRA-2 and M2AMIP patterns that were selected for the NAO, characterized by lower sea level pressure over Greenland and higher sea level pressure to the south during the positive phase, can be seen in Figure 2.5.1. These are the leading patterns for both datasets, explaining 43.7% of the monthly mean variance in MERRA-2 and 40.3% in M2AMIP. The anomalies are stronger, however, in MERRA-2 than in M2AMIP. For both MERRA-2 and M2AMIP, the centers of the negative anomaly in sea level pressure are located along the

southeast coast of Greenland, and the positive anomalies are northwest of Spain. The time series of the NAO index from MERRA-2 and M2AMIP can be found in panel d of the figures in section 3.3.

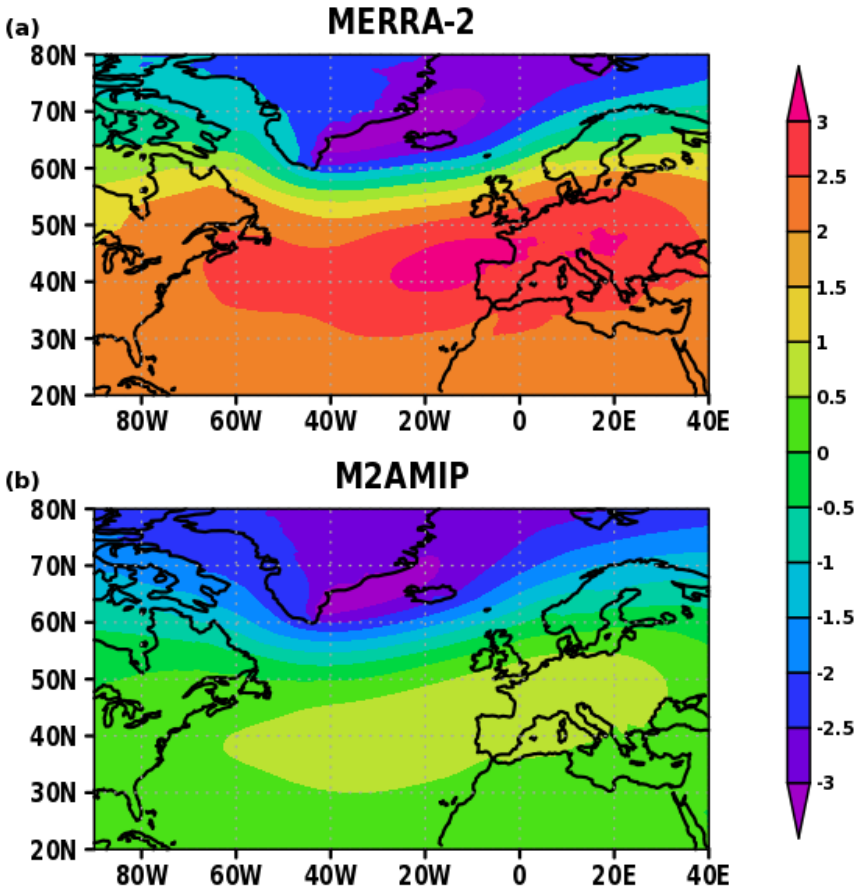

Figure 2.5.1: The selected REOF depicting the NAO during DJF for (a) MERRA-2 and (b) M2AMIP.

The REOF for the PNA is based on monthly mean 250 hPa heights within the entire northern hemisphere. The positive phase of the PNA is characterized by above-average heights in the northwestern United States and below-average heights in the eastern United States, as seen in the selected REOF patterns for MERRA-2 and M2AMIP (Figure 2.5.2). The fraction of monthly mean variance explained by this leading pattern is 19.2% in MERRA-2 and 23.6% in M2AMIP.

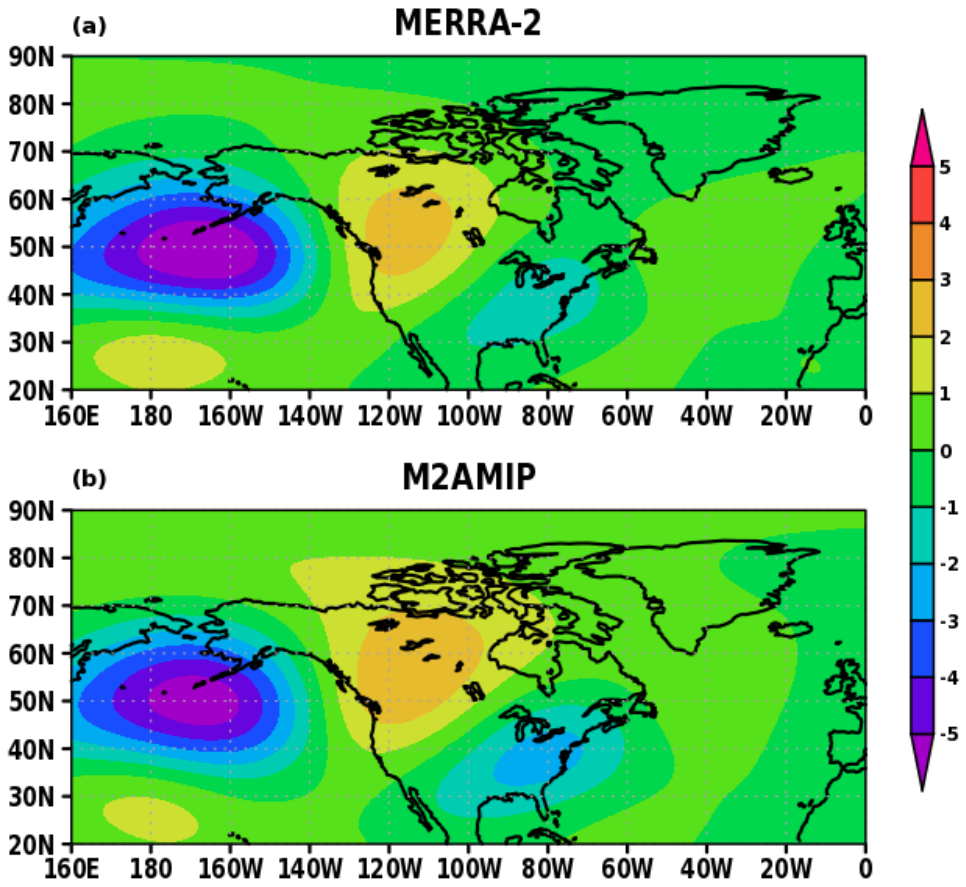

Figure 2.5.2: The selected REOF depicting the PNA for (a) MERRA-2 and (b) M2AMIP.

2.6 Extreme Event Indices

A threshold-based approach is used to identify extreme events for both temperature and precipitation. First, Cumulative Distribution Functions (CDFs, using 40 bins) of precipitation, minimum temperature, and maximum temperature were determined for every day of the year, for each grid cell (or temperature observation station) using data from the climatology period of 1981 through 2010. In an effort to account for day-to-day variability, which is strong for precipitation, a 15-day running window centered on the date in question was in fact used to derive the CDFs from the MERRA2, CPCU and GHCN data. For M2AMIP, data across all ensemble members from the 30-year period within a 3-day window centered on the day in question are included individually to compute the CDF – the ensemble mean time series was not used.

For the precipitation CDF calculation, only days with at least 1 mm of precipitation were considered, a standard practice for precipitation studies. Note that the number of days considered can differ between the three datasets (Figures 2.6.1 through 2.6.4). In general, the spatial patterns of the number of days with rain in M2AMIP, MERRA-2, and the observations

are similar; however, M2AMIP has too few days with precipitation in the Northwest and the Northern Great Plains and too many days in the Northeast. In JJA, M2AMIP has too few days with precipitation in the western two-thirds of the country and too many days with precipitation along the east coast.

An extreme event is said to occur if the minimum temperature, maximum temperature or precipitation exceeds (or is below, in the case of cold extremes) the percentile in question. The resulting extreme event indices, representing the frequency or intensity of events, are based on the indices set forth by the Expert Team on Climate Change Detection and Indices (ETCCDI) and are described in Table 1 of Alexander (2015). A subset of these indices, including those evaluated here, can be found in Table 2.1.

Table 2.1 Extreme temperature and precipitation indices

Index	Description	Units
PRCPTOT	Total precipitation on days exceeding 1 mm	mm
R99P	Precipitation on days that exceed the 99th percentile	mm
R99D	Number of days that exceed the 99th percentile of precipitation	Days
T2M	Daily mean 2 m temperature	K
TX90p	Percentage of time daily maximum temperature exceeds the 90th percentile	%
TN10p	Percentage of time daily minimum temperature is below the 10th percentile	%

Within this set of indices are metrics that relate to the mean state (PRCPTOT and T2M) as well as the frequency (R99D, TX90P, and TN10P) and intensity (R99P) of extreme weather events. The percentile-based indices for the frequency of extreme weather events do not necessarily indicate that the event occurs ten percent of the time for TX90P and TN10P or one percent of the time for R99D, given that the samples going into the percentile calculation were limited to the climatology period of 1981 through 2010 and to only include days with precipitation (Figures 2.6.1 to 2.6.4) – if all days were considered (including rain-free days), the fraction of time associated with the extremes would in fact be less than 10% or 1%. Of key importance here is the interannual variability within these indices.

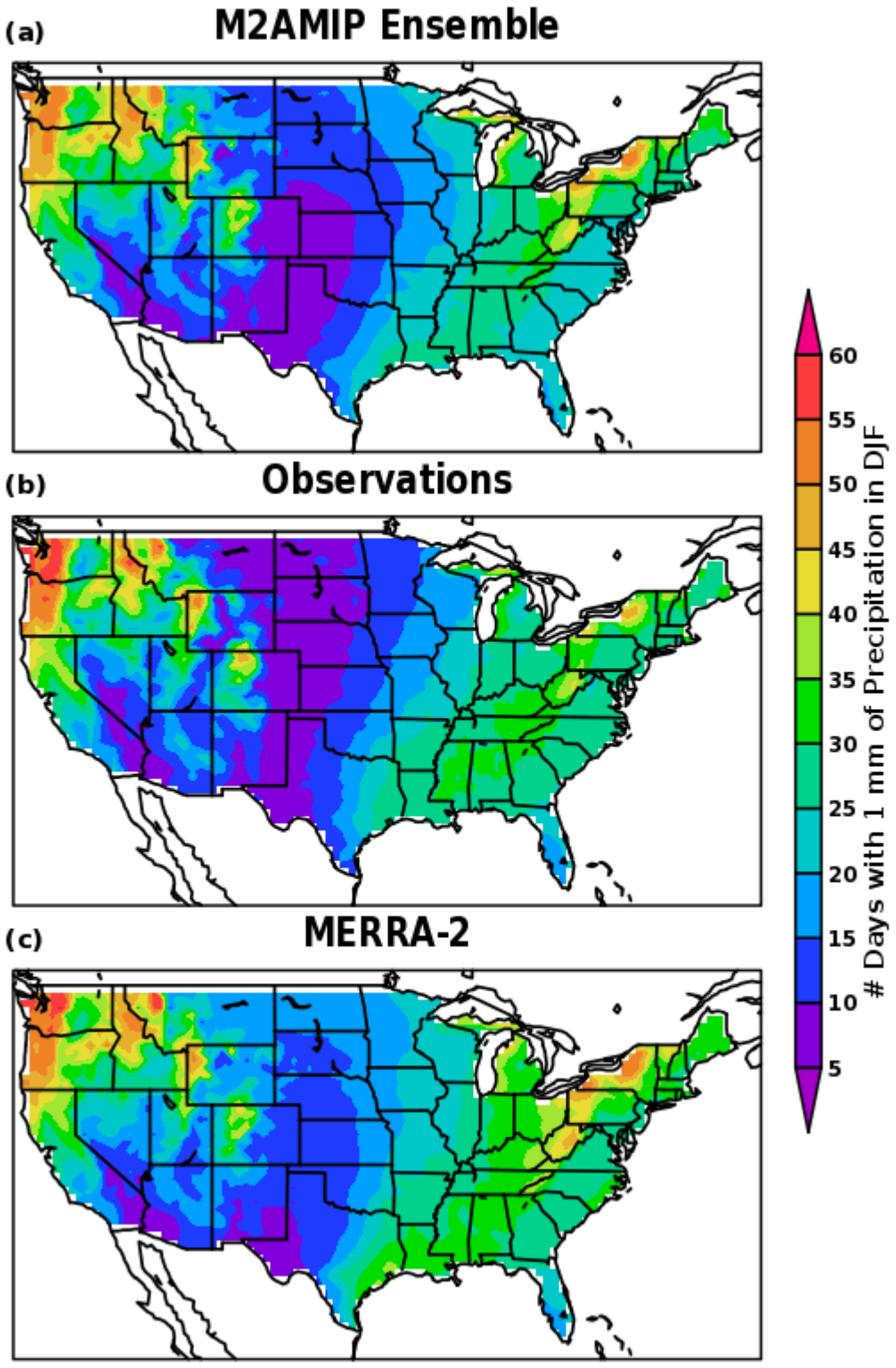

Figure 2.6.1: Average number of days in DJF with at least 1 mm of precipitation in (a) M2AMIP, (b) observations, and (c) MERRA-2.

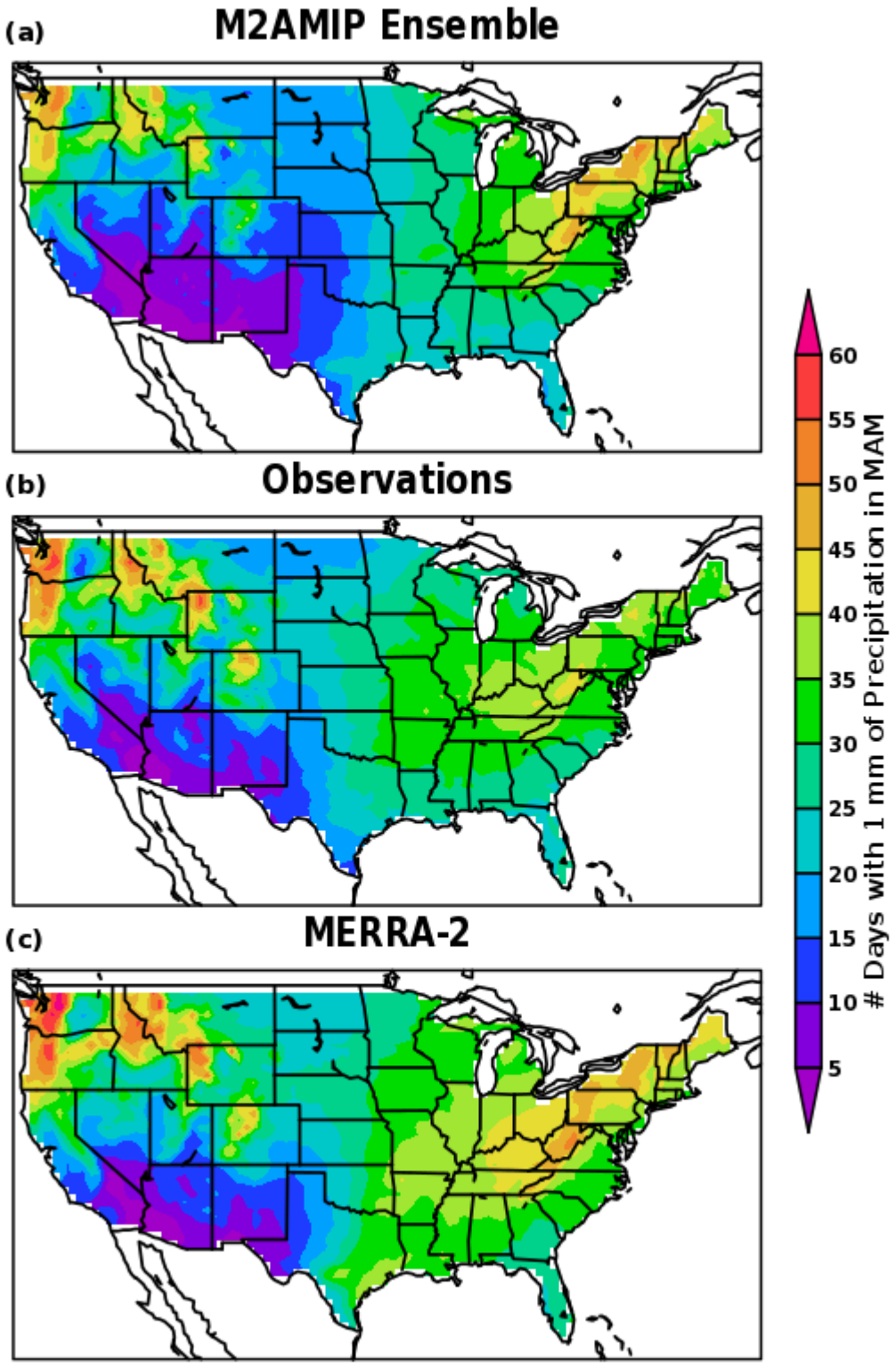

Figure 2.6.2: Average number of days in MAM with at least 1 mm of precipitation in (a) M2AMIP, (b) observations, and (c) MERRA-2.

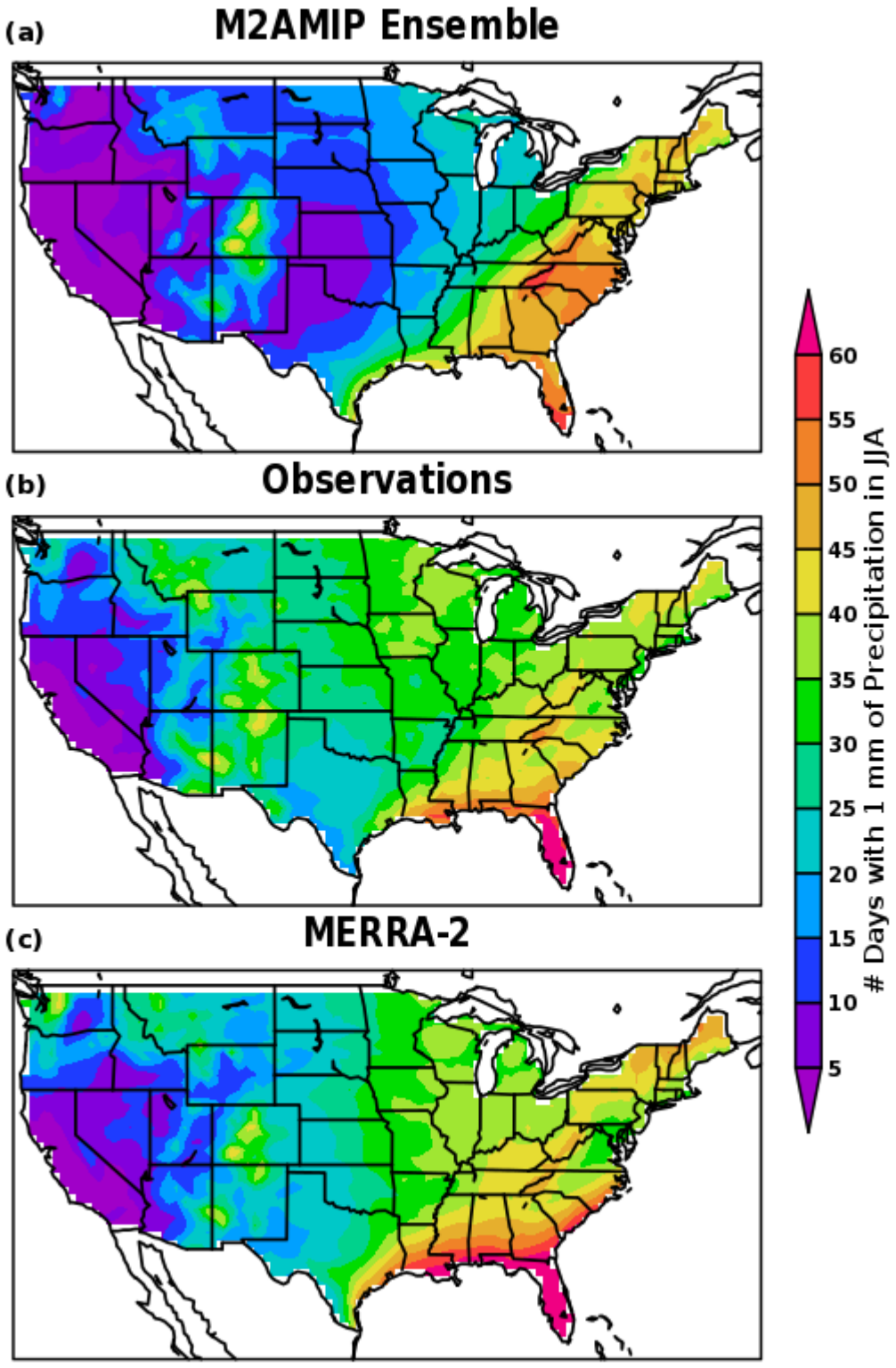

Figure 2.6.3: Average number of days in JJA with at least 1 mm of precipitation in (a) M2AMIP, (b) observations, and (c) MERRA-2.

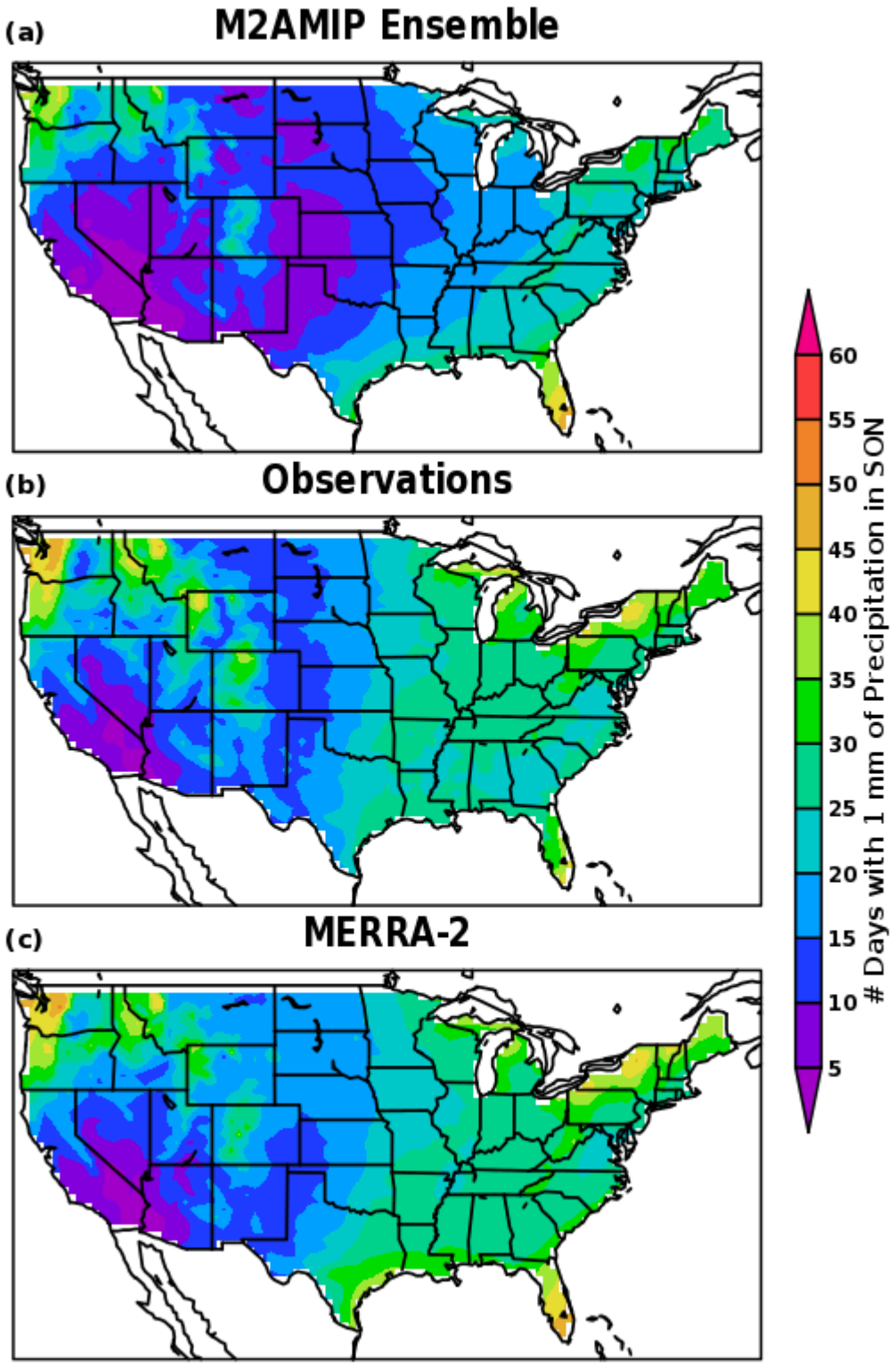

Figure 2.6.4: Average number of days in SON with at least 1 mm of precipitation in (a) M2AMIP, (b) observations, and (c) MERRA-2.

3. Results

Correlations between seasonal, for ENSO and the PDO, and monthly, for the NAO and PNA, climate indices (i.e., teleconnection patterns, section 2.5) and indices associated with precipitation and temperature (Table 2.1) over the United States National Climate Assessment (NCA) domain were computed from the 36 years of data separately for each season. This section highlights noteworthy correlations uncovered in the analysis. Note that some teleconnection patterns are not significantly correlated to weather in the US, particularly in the summer months. Given the large number of correlations explored, we cannot present all of the results here. The entire collection of figures can be found in the supplemental online library at https://gmao.gsfc.nasa.gov/multi-partner/NCA/pubs/TM47_suppl/.

In the following, each figure contains six panels. The left column shows the correlations between the climate index and the temperature or precipitation index for M2AMIP, observations, and MERRA-2 in the top row, middle, and bottom rows, respectively. The right column shows the correlation between the climate index and the 500 hPa heights in M2AMIP and MERRA-2 as well as a time series of the climate index. The color bar values represent correlations that are, for the observations and MERRA-2, statistically different from zero at the 90%, 95%, and 99% confidence levels. Since the M2AMIP results are based on ten times more data (10 ensemble members), the 99% confidence level occurs at a lower correlation coefficient; thus, the 99% confidence level is shown with contours in the M2AMIP panels.

3.1 El Niño/Southern Oscillation

ENSO is a coupled mode of variability of the atmosphere-ocean system. A weakened or reversed Walker circulation during the positive phase, or El Niño, prevents the upwelling of cool ocean water, allowing for above-average sea surface temperatures in the central Pacific, whereas below-average sea surface temperatures are present during La Niña, the negative phase of ENSO. These changes in the Pacific Ocean are capable of influencing weather around the globe. For additional information on ENSO, we refer the reader to the Climate Prediction Center's website on ENSO, http://www.cpc.ncep.noaa.gov/products/precip/CWlink/MJO/enso.shtml.

The most substantial influence of ENSO on temperature and precipitation in the United States occurs during DJF. The Niño3.4 index has a statistically significant positive correlation with the total seasonal precipitation (on days with at least 1 mm of precipitation) in the southern portion of the country and a negative correlation over the Great Lakes and the Montana area (Figure 3.1.1). This pattern can be seen in the observations, MERRA-2, and M2AMIP, with excellent agreement between the observations and MERRA-2 (Figures 3.1.1c and e). M2AMIP extends the positive correlation up the east coast and the negative correlation in the northwest to the Pacific coast (Figure 3.1.1a); however, given the differences between MERRA-2 and M2AMIP in the 500 hPa-Niño3.4 correlations, this is not unreasonable (Figures 3.1.1b and f). In general, positive correlations between precipitation and Niño3.4 are seen where there is a negative correlation between 500 hPa height and Niño3.4 and vice versa, likely due to increased

storminess along a trough across the country. The negative correlation between DJF Niño3.4 and 500 hPa height in M2AMIP has a northeastward tilt extending from the southwestern to the northeastern part of the US while MERRA-2 does not have a negative correlation further north or east than South Carolina (Figures 3.1.1b and f). In a similar manner, the positive correlation between DJF Niño3.4 and 500 hPa height extends further to the west in M2AMIP than in MERRA-2. Wet conditions along the southern portion of the country during El Niño conditions have previously been documented in the literature. In fact, our results for the correlation between Niño3.4 and total precipitation are very similar to those shown in Figure 1 of Wise et al. (2015), which depicts the correlation between cool season standardized precipitation and the Southern Oscillation Index.

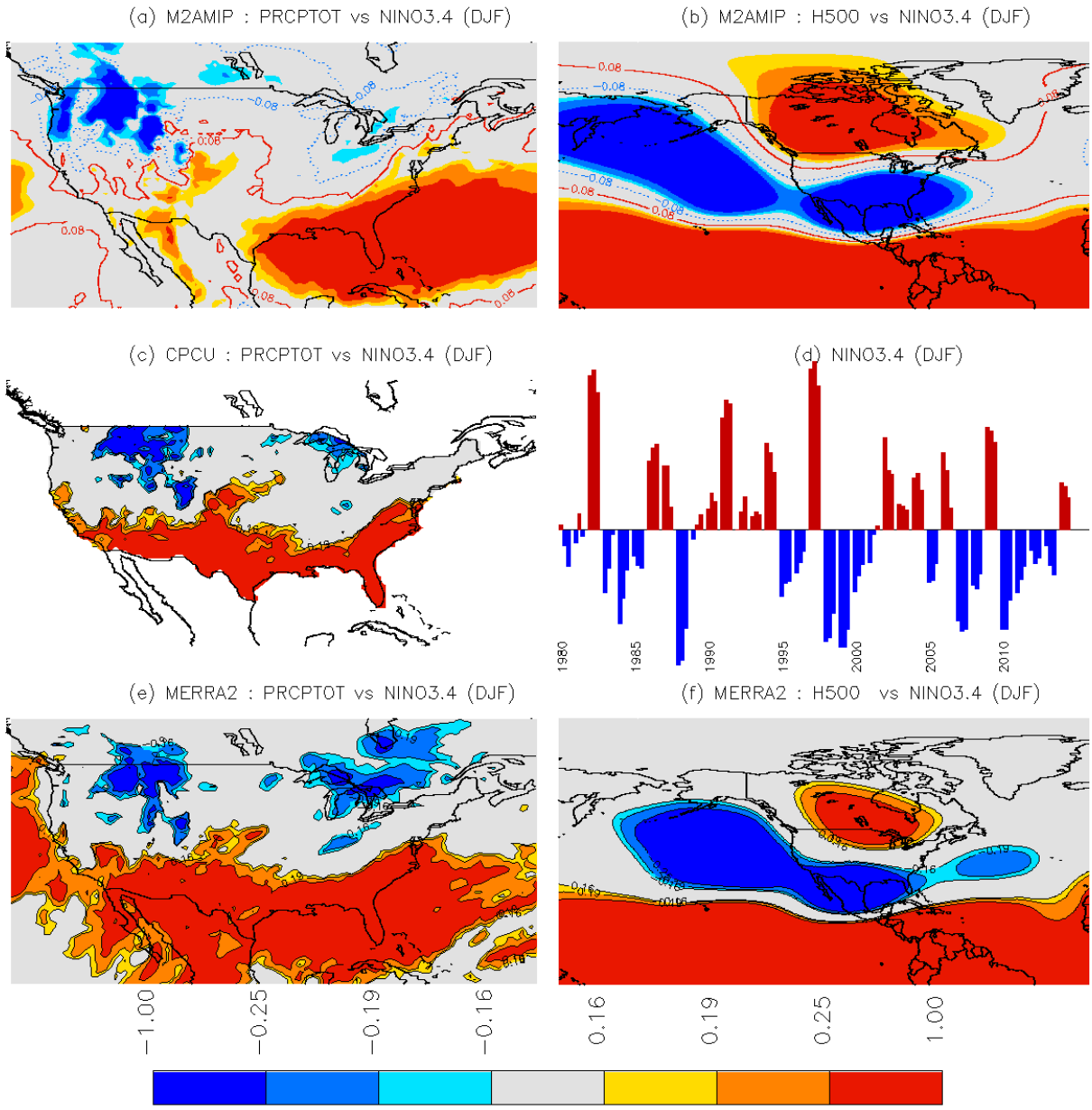

Figure 3.1.1: DJF (a) correlation between Niño3.4 and M2AMIP total precipitation, (b) correlation between Niño3.4 and 500 hPa heights in M2AMIP, (c) correlation between Niño3.4 and observed total precipitation, (d) time series of the Niño3.4 index, (e) correlation between Niño3.4 and MERRA-2 precipitation, and (f) correlation between Niño3.4 and 500 hPa heights in MERRA-2.

Significant correlations with Niño3.4 during DJF are also found for extreme precipitation events defined in terms of the 90th, 95th, and 99th percentiles. The correlation between DJF precipitation associated with events at the 99th percentile is shown as an example in Figure 3.1.2; figures for the 90th and 95th percentiles can be found in the online supplementary library. The spatial patterns of the correlations are roughly the same for extreme precipitation as for total precipitation, though the correlations decrease in magnitude as the precipitation percentile increases (Figures 3.1.2a, c, and e). This can signify that ENSO conditions shift the entire PDF of precipitation. The positive correlation between DJF Niño3.4 and R99P somewhat falls apart in the southwest and Great Plains in MERRA-2 and M2AMIP; the areas with significant correlations are more scattered in MERRA-2 than in the observations and are essentially non-existent in M2AMIP. A likely explanation for the lack of agreement in the western portion of the country is that there are only on average a handful of days that see at least 1 mm of precipitation in a given season (Figure 2.6.1).

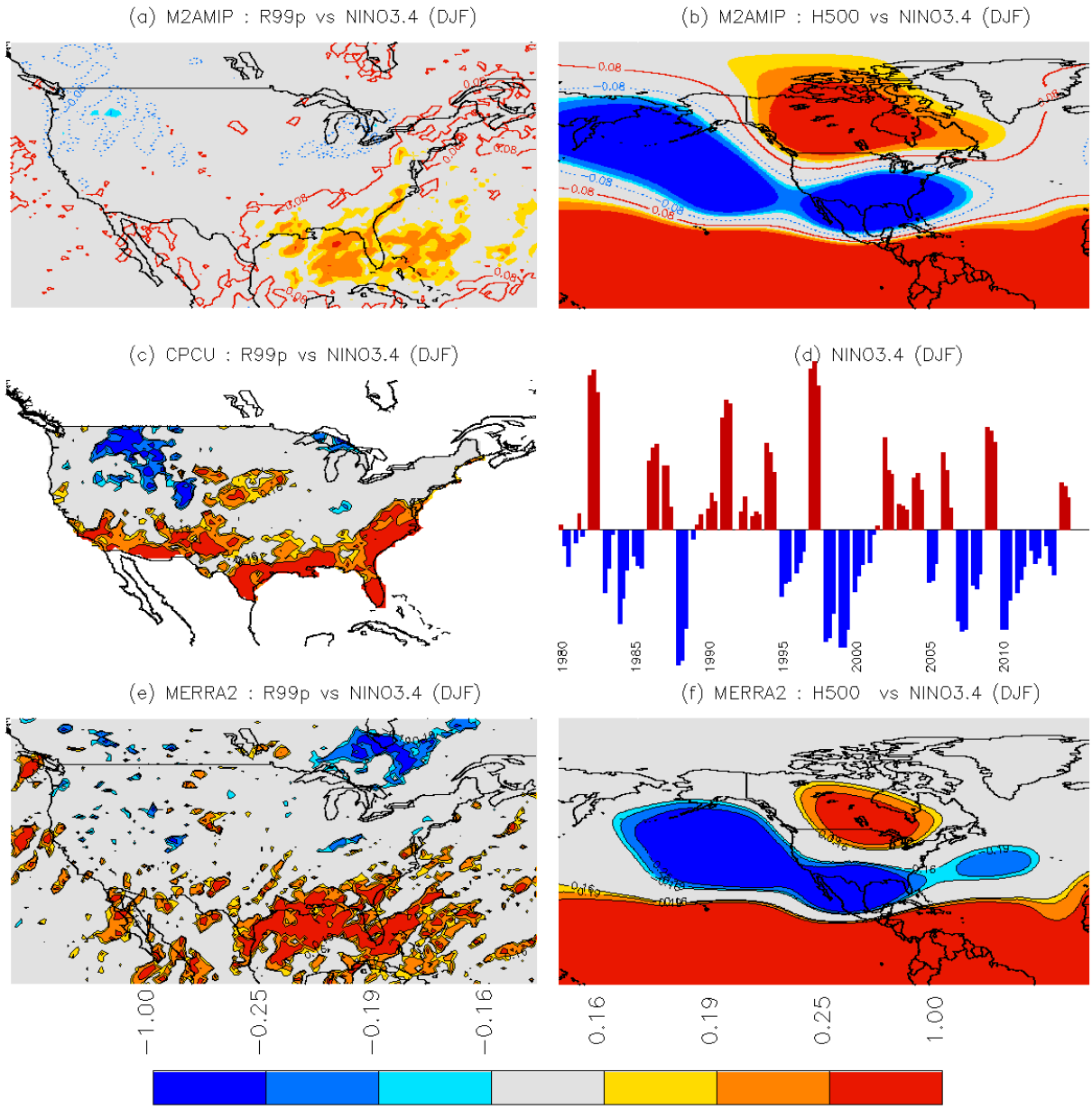

Figure 3.1.2: DJF (a) correlation between Niño3.4 and M2AMIP R99P, (b) correlation between Niño3.4 and 500 hPa heights in M2AMIP, (c) correlation between Niño3.4 and observed R99P, (d) time series of the Niño3.4 index, (e) correlation between Niño3.4 and MERRA-2 R99P, and (f) correlation between Niño3.4 and 500 hPa heights in MERRA-2.

The correlation pattern between Niño3.4 and the frequency of 99th percentile precipitation events is also similar to that for total precipitation. The observations show a positive correlation between DJF Niño3.4 and the frequency of 99th percentile events in the southern portion of the country, along a strip extending from Arizona to Texas as well as in Florida (Figure 3.1.3c). The teleconnection in Florida is picked up in MERRA2 and M2AMIP, along with a larger portion of the southeast; in the case of M2AMIP, the significant correlations extend up the entire east coast (Figures 3.1.3a and e). However, the teleconnection between Arizona and Texas is absent in both MERRA-2 and M2AMIP. Similarly, the negative correlation observed in the Montana and Great Lakes regions is also not present in MERRA-2. M2AMIP has a hint of the negative correlation in the Great Lakes region, as well as negative correlations to the west of the Montana area. Conversely, MERRA-2 and M2AMIP show a correlation along the Gulf Coast between Alabama and Louisiana that is not present in the observations. The observed correlations for the frequency and intensity of extreme precipitation events presented here are very similar to those presented in Figures 6d and 6h of Mallakpour and Villarini (2016a).

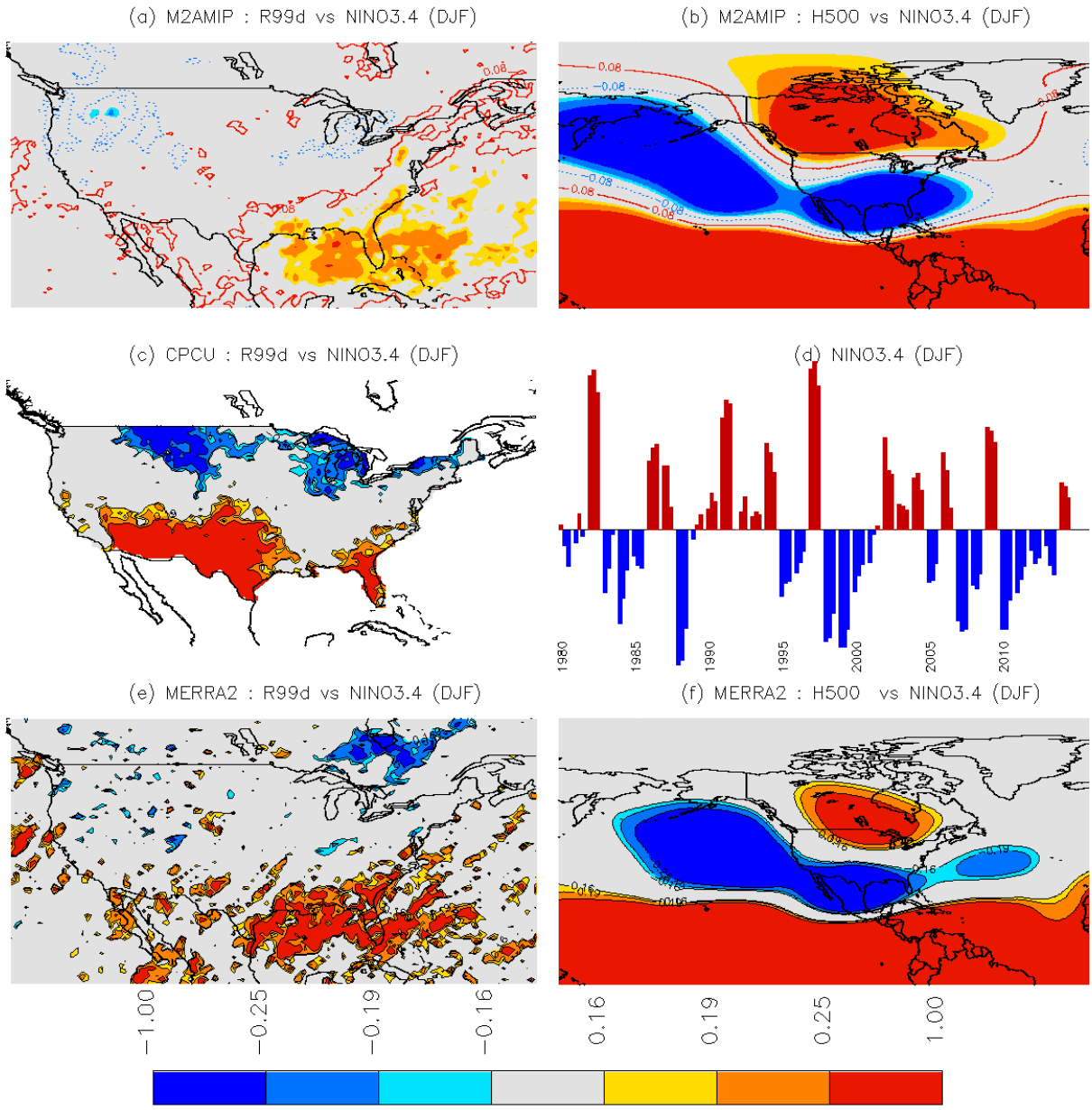

Figure 3.1.3: DJF (a) correlation between Niño3.4 and M2AMIP R99D, (b) correlation between Niño3.4 and 500 hPa heights in M2AMIP, (c) correlation between Niño3.4 and observed R99D, (d) time series of the Niño3.4 index, (e) correlation between Niño3.4 and MERRA-2 R99D, and (f) correlation between Niño3.4 and 500 hPa heights in MERRA-2.

The spatial patterns of the temperature correlations to Niño3.4 are similar to those for precipitation. Areas that see enhanced precipitation also see cooler temperatures, whereas areas with suppressed precipitation experience warmer temperatures. This makes sense because a moist surface will expend energy to evaporate water rather than heat the surface. A negative correlation between Niño3.4 and TX90P, or the percentage of days that exceed the 90th percentile of maximum 2 m temperature, can be seen across the southern portion of the country in areas that also show a negative correlation with precipitation (Figures 3.1.4a, c, and e). A reduction in temperature in the southern United States during El Niño conditions is indeed documented in the literature (e.g., Dourte at al., 2016) and has previously been shown to be primarily due to a reduction in downwelling shortwave radiation as a result of enhanced cloud cover (Zhang et al., 2011). Good agreement can be seen between the observations and MERRA-2; however, as was found for the precipitation correlations, the positive Niño3.4-TX90P correlations in M2AMIP extend further to the northeast, as the correlation in 500 hPa height is also shifted in that direction in M2AMIP (Figure 3.1.4b). A statistically significant positive correlation can be seen in the northwest region of the United States in all three data sets (Figures 3.1.4a, c, and e).

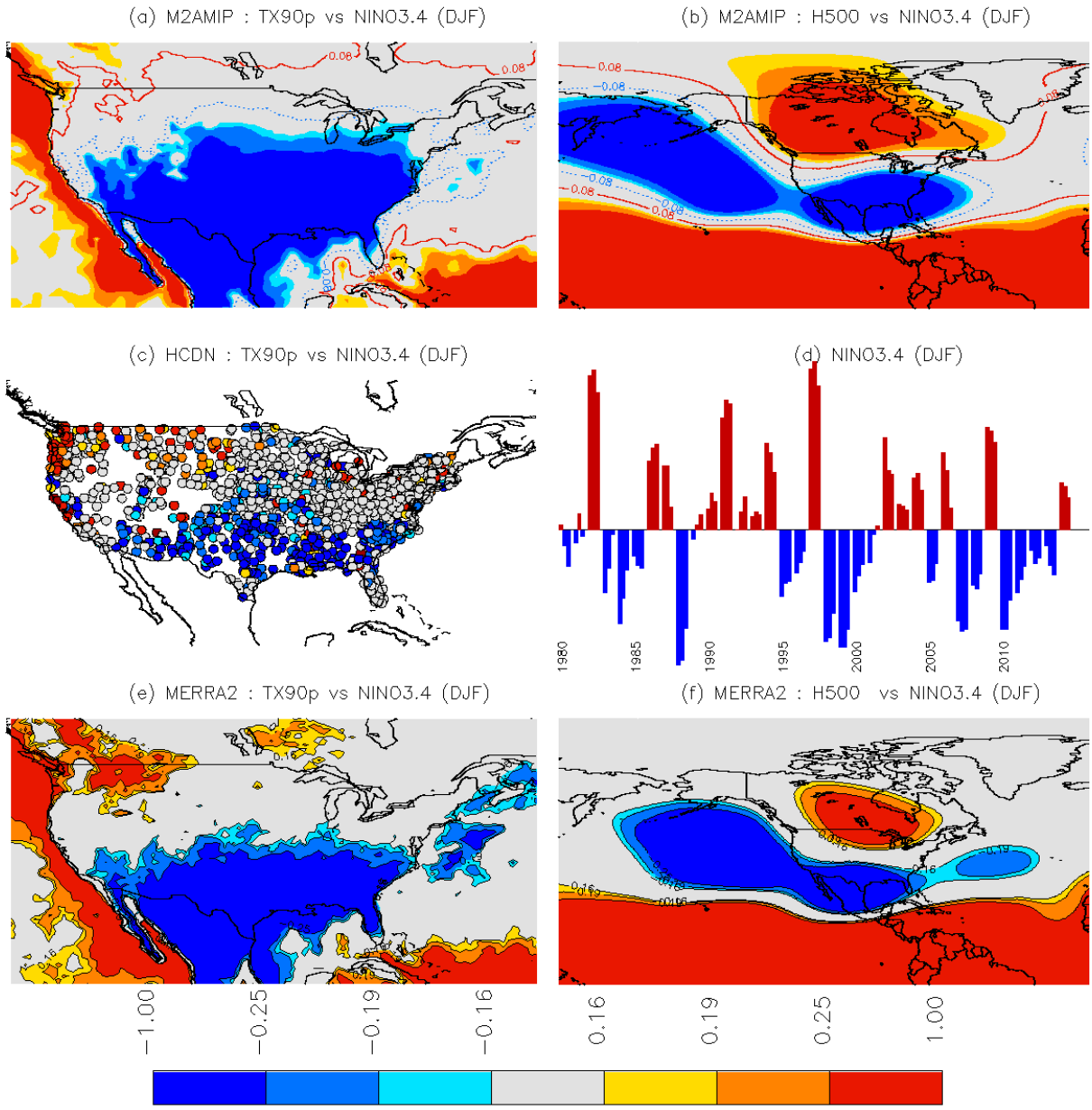

Figure 3.1.4: DJF (a) correlation between Niño3.4 and M2AMIP TX90P, (b) correlation between Niño3.4 and 500 hPa heights in M2AMIP, (c) correlation between Niño3.4 and observed TX90P, (d) time series of the Niño3.4 index, (e) correlation between Niño3.4 and MERRA-2 TX90P, and (f) correlation between Niño3.4 and 500 hPa heights in MERRA-2.

Correlations to Niño3.4 are weaker and less widespread in the other seasons, but there are regions of the United States that see statistically significant correlations between Niño3.4 and precipitation, temperature, and 500 hPa heights (see online supplemental library). For example, the statistically significant negative correlation between DJF precipitation and Niño3.4 in the southern portion of the country continues into MAM in all three datasets, though the relationship is weaker. There is also a pronounced negative correlation in the observations between MAM Niño3.4 and the frequency of extreme precipitation events in the southwestern United States, a teleconnection that is not present in MERRA-2 or M2AMIP.

Statistically significant correlations with mean and extreme precipitation in JJA are confined to the northwestern US and are present in both MERRA-2 and the observations; however, M2AMIP struggles to represent this relationship (Figure 3.1.5). A positive relationship between precipitation and ENSO in the northwest during JJA, spanning the region from eastern Oregon to western South Dakota, has previously been documented in the literature. Barlow et al. (2001) shows this relationship, particularly during the month of August, based on observations, while Bosilovich (2013) found a positive correlation between JJA precipitation and MAM Niño3.4 in the same region. However, Yoon and Leung (2015) caution that warm season precipitation can be affected more by antecedent precipitation and soil moisture than by ENSO in this region. If M2AMIP incorrectly lacked MAM precipitation in years that El Niño conditions developed in JJA, precipitation may be reduced in the summer months due to a lack of surface-induced moisture availability (a problem MERRA-2 wouldn't face, given the use therein of observations-corrected precipitation to force the land surface). It is also worth noting that there are fewer days in JJA with precipitation in the western half of the US in M2AMIP compared to either MERRA-2 or the observations (Figure 2.6.3), which could impact the precipitation statistics.

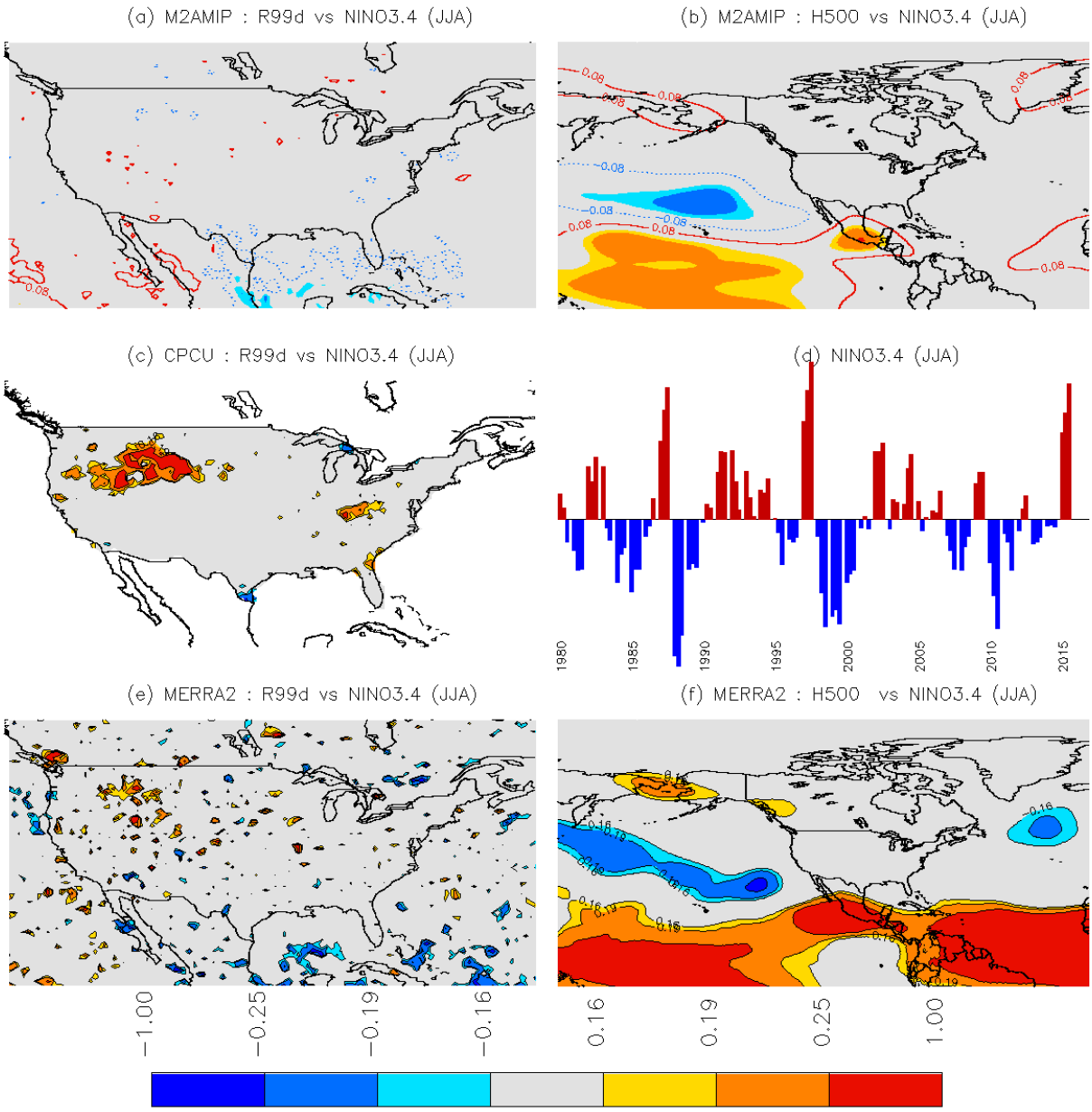

Figure 3.1.5: JJA (a) correlation between Niño3.4 and M2AMIP R99D, (b) correlation between Niño3.4 and 500 hPa heights in M2AMIP, (c) correlation between Niño3.4 and observed R99D, (d) time series of the Niño3.4 index, (e) correlation between Niño3.4 and MERRA-2 R99D, and (f) correlation between Niño3.4 and 500 hPa heights in MERRA-2.

An interesting example of correlations between Niño3.4 and extreme temperature events can be seen in SON. There is essentially no statistically significant relationship between daily mean 2 m temperature and the Niño3.4 index anywhere in the US in MERRA-2, M2AMIP, or the observations (Figure 3.1.6a, c, and e). Despite this, there is a statistically significant negative correlation in the central United States between Niño3.4 and the frequency of days with a maximum temperature exceeding the 90th percentile (Figure 3.1.7a, c, and e). The spatial pattern of this correlation does not entirely agree between the three datasets, but they all show some correlation, particularly around Colorado. MERRA-2 and the observations extend the correlation to the east, while M2AMIP extends it to the Northeast, reaching the Great Lakes. While the literature does not contain many examples of the relationship between ENSO and extreme temperature events during SON, Table 5 of Wolter et al. (1999) shows 18% of the contiguous United States has a statistically significant increased risk of an extreme temperature event (warm or cold) during El Niño conditions in SON. This number jumps to 46% with a one season lead time (JJA El Niño conditions in relation to SON events), which is the largest area presented for all lead times and seasons (Wolter et al., 1999).

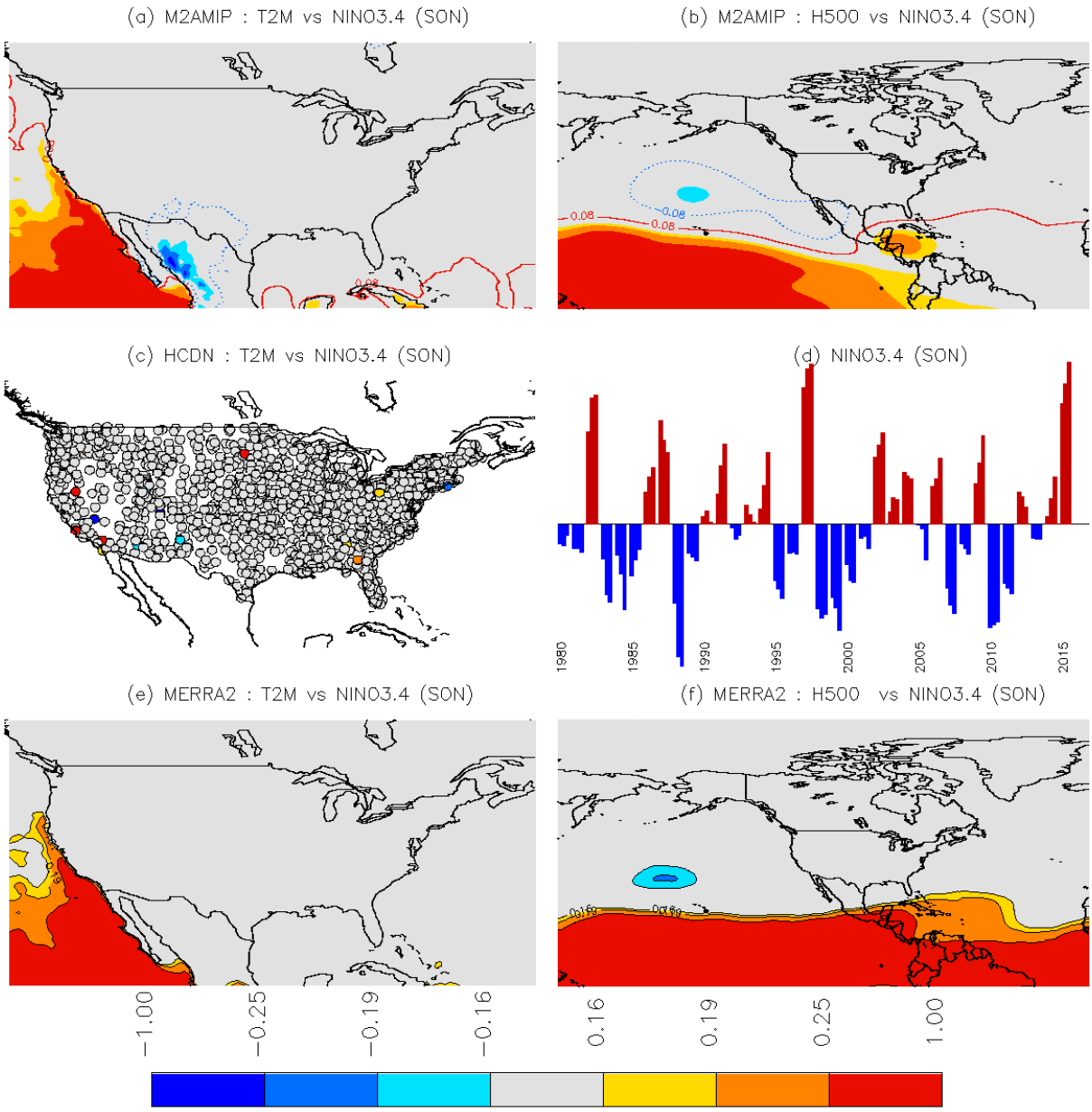

Figure 3.1.6: SON (a) correlation between Niño3.4 and M2AMIP daily mean 2 m temperature, (b) correlation between Niño3.4 and 500 hPa heights in M2AMIP, (c) correlation between Niño3.4 and observed daily mean 2 m temperature, (d) time series of the Niño3.4 index, (e) correlation between Niño3.4 and MERRA-2 daily mean 2 m temperature, and (f) correlation between Niño3.4 and 500 hPa heights in MERRA-2.

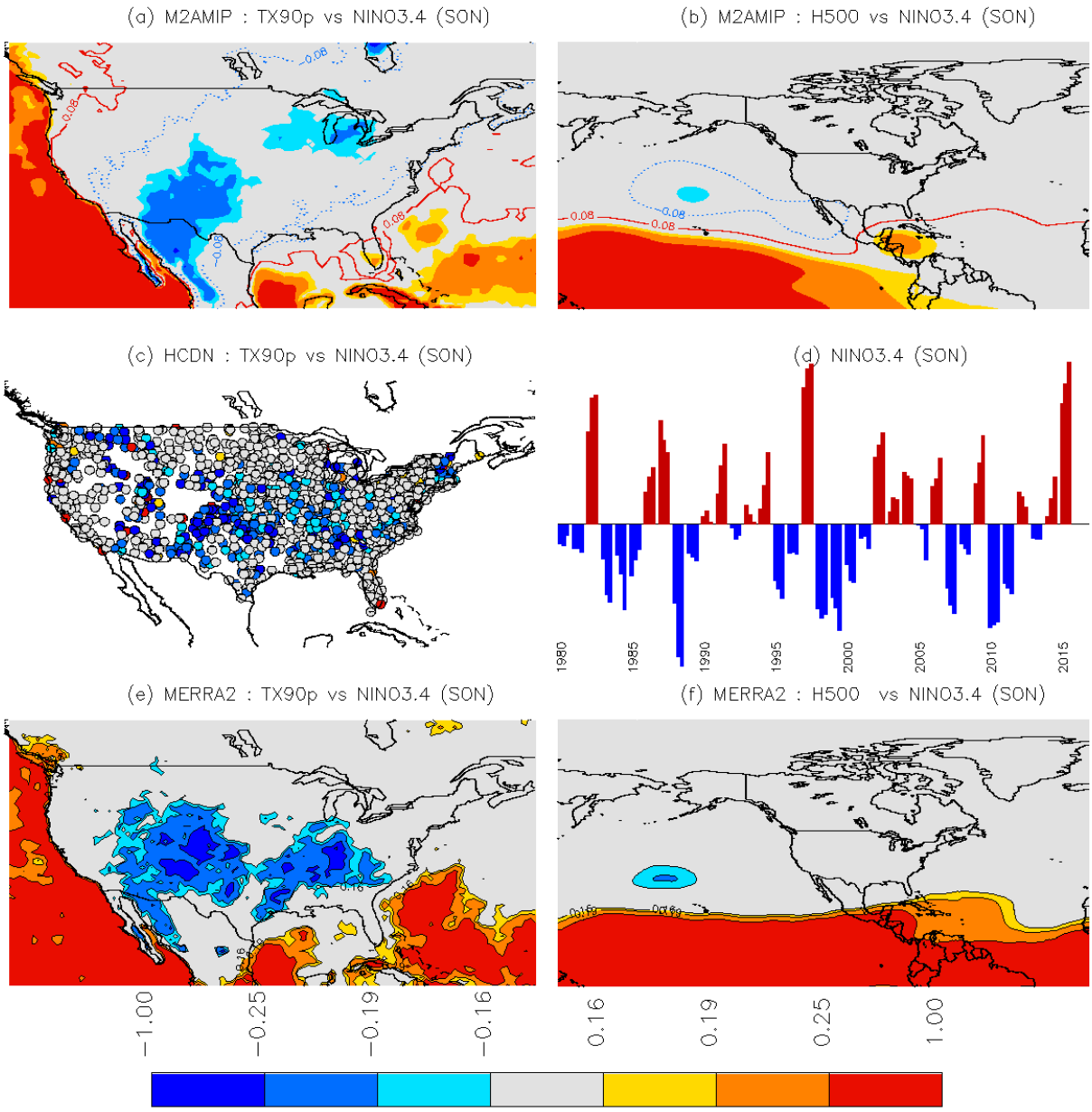

Figure 3.1.7: SON (a) correlation between Niño3.4 and M2AMIP TX90P, (b) correlation between Niño3.4 and 500 hPa heights in M2AMIP, (c) correlation between Niño3.4 and observed TX90P, (d) time series of the Niño3.4 index, (e) correlation between Niño3.4 and MERRA-2 TX90P, and (f) correlation between Niño3.4 and 500 hPa heights in MERRA-2.

3.2 Pacific Decadal Oscillation

The warm phase of the PDO is characterized by above-average sea surface temperatures along the west coast of the Americas alongside cool sea surface temperatures in the central North Pacific and a deepening of the Aleutian low, with the reverse pattern during the cool phase (Mantua and Hare, 2002). The warm phase sea surface temperature dipole results in high sea level pressure in the western tropical Pacific and low sea level pressure in the eastern tropical Pacific, and these atmospheric anomalies extend into the upper troposphere (Mantua and Hare, 2002). Additional details on the PDO can be found in the recent review article by Newman et al. (2016).

The teleconnections in the US associated with the PDO are similar to those associated with ENSO, and as a result, many studies aim to isolate the influences of the two (Newman et al., 2016). As with ENSO, correlations between the PDO and 500 hPa heights are strongest in the wintertime. Negative correlations with 500 hPa heights are centered in the southeast United States, with the statistically significant region spanning from Texas to Massachusetts in MERRA-2 (Figure 3.2.1f). This negative correlation is still present in MAM, though the correlations are smaller in magnitude (Figure 3.2.2f). Also for MERRA-2, a region of statistically significant positive correlations with 500 hPa heights during DJF is located in the Northwest, extending into Alberta and eastern British Columbia, Canada (Figure 3.2.1).

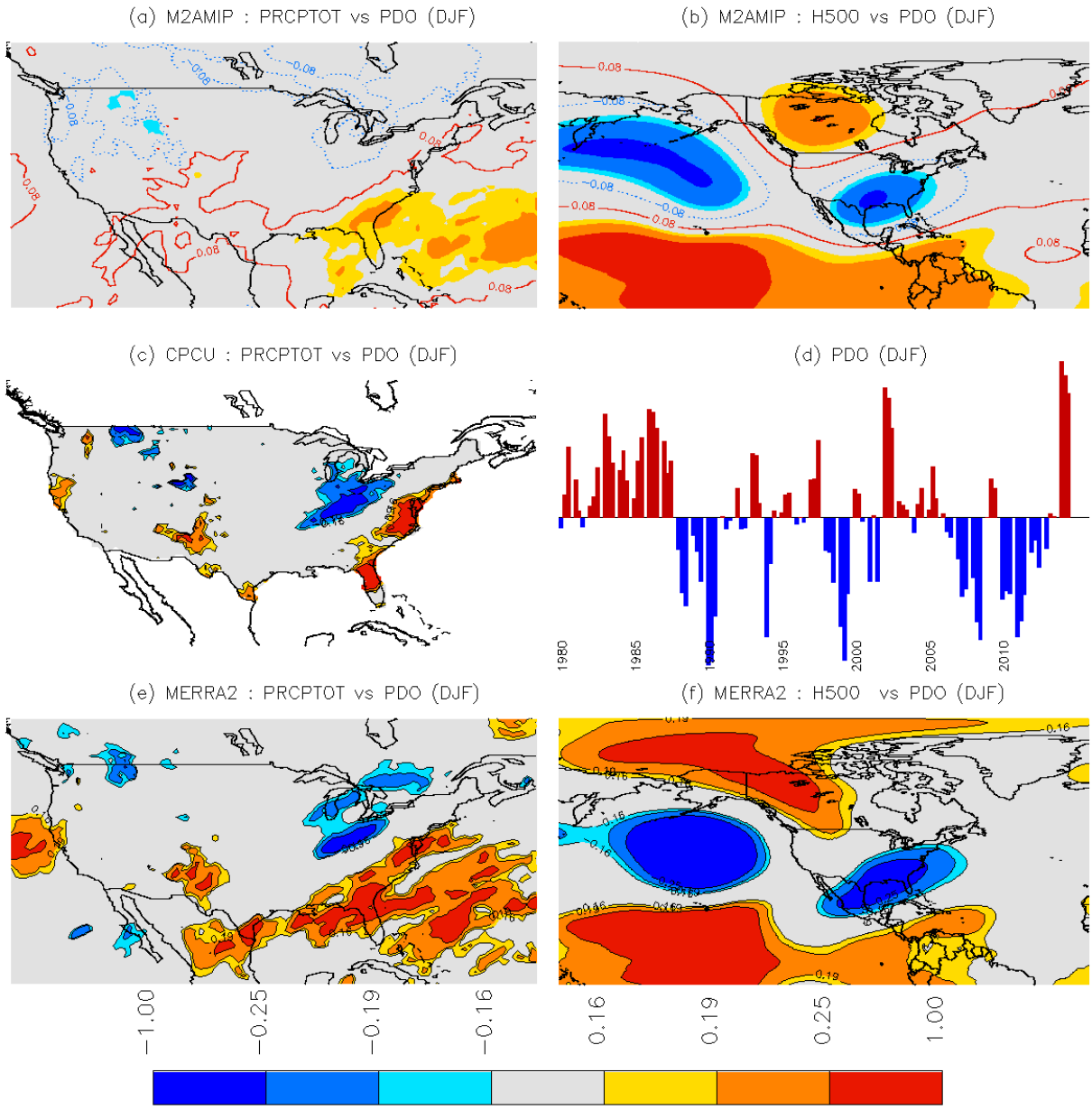

Figure 3.2.1: DJF (a) correlation between PDO index and M2AMIP total precipitation, (b) correlation between PDO index and 500 hPa heights in M2AMIP, (c) correlation between PDO index and observed total precipitation, (d) time series of the PDO index, (e) correlation between PDO index and MERRA-2 precipitation, and (f) correlation between PDO index and 500 hPa heights in MERRA-2.

The negative correlation for DJF between PDO and 500 hPa heights is accompanied by a positive correlation with total and extreme precipitation in the southeast US in MERRA-2, M2AMIP, and the observations (Figures 3.2.1a, c, and e). Due to the similarity between the correlations for total precipitation and for the intensity of 90^{th}, 95^{th}, and 99^{th} percentile precipitation events, the figures for extreme precipitation are not included here but can be viewed in the online supplemental library.

Precipitation in the other seasons in relation to the PDO is a bit more troublesome for MERRA-2 and M2AMIP. Although statistically significant correlations are seen in the observations, neither MERRA-2 nor M2AMIP show a coherent region of statistically significant correlation for extreme precipitation. Figure 3.2.2 shows results for the MAM 99^{th} percentile events. (These results are representative of problems seen; there are also issues in JJA and SON for total precipitation and for the 90^{th} and 95^{th} percentile events.) In the observations, there is a negative correlation between the MAM PDO and the intensity of 99^{th} percentile precipitation events from the Great Lakes to northeast Texas (Figure 3.2.2c). MERRA-2 shows a hint of this negative correlation; however, a clear signal is absent (Figure 3.2.2e). M2AMIP shows no evidence at all of this relationship (Figure 3.2.2c). MERRA-2 and M2AMIP similarly fail to reproduce the observed statistically significant positive correlation between the MAM PDO and the frequency of 99^{th} percentile events in the southwestern and northeastern US (Figures 3.2.3 a, c and e).

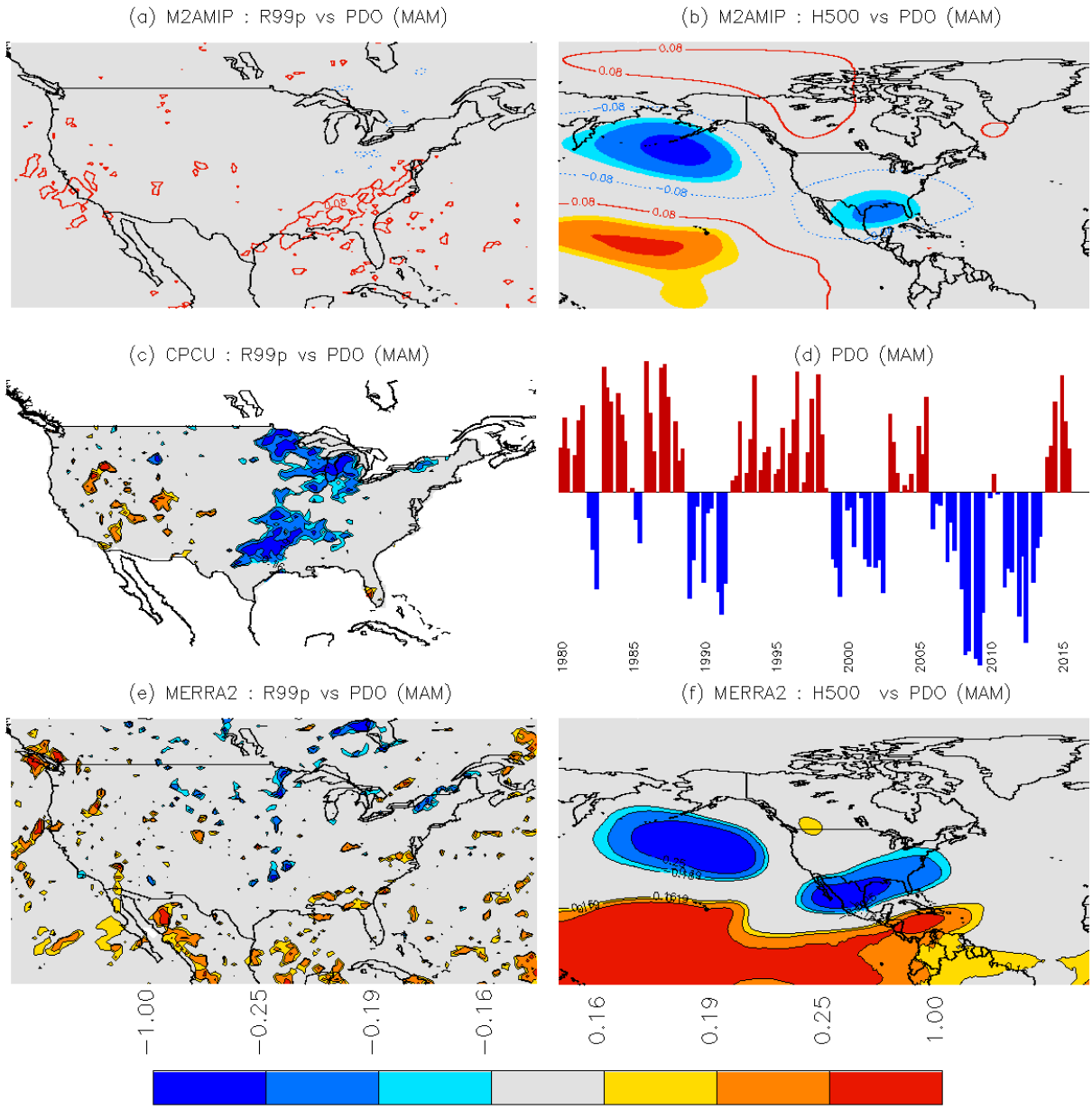

Figure 3.2.2: MAM (a) correlation between PDO index and M2AMIP R99P, (b) correlation between PDO index and 500 hPa heights in M2AMIP, (c) correlation between PDO index and observed R99P, (d) time series of the PDO index, (e) correlation between PDO index and MERRA-2 R99P, and (f) correlation between PDO index and 500 hPa heights in MERRA-2.

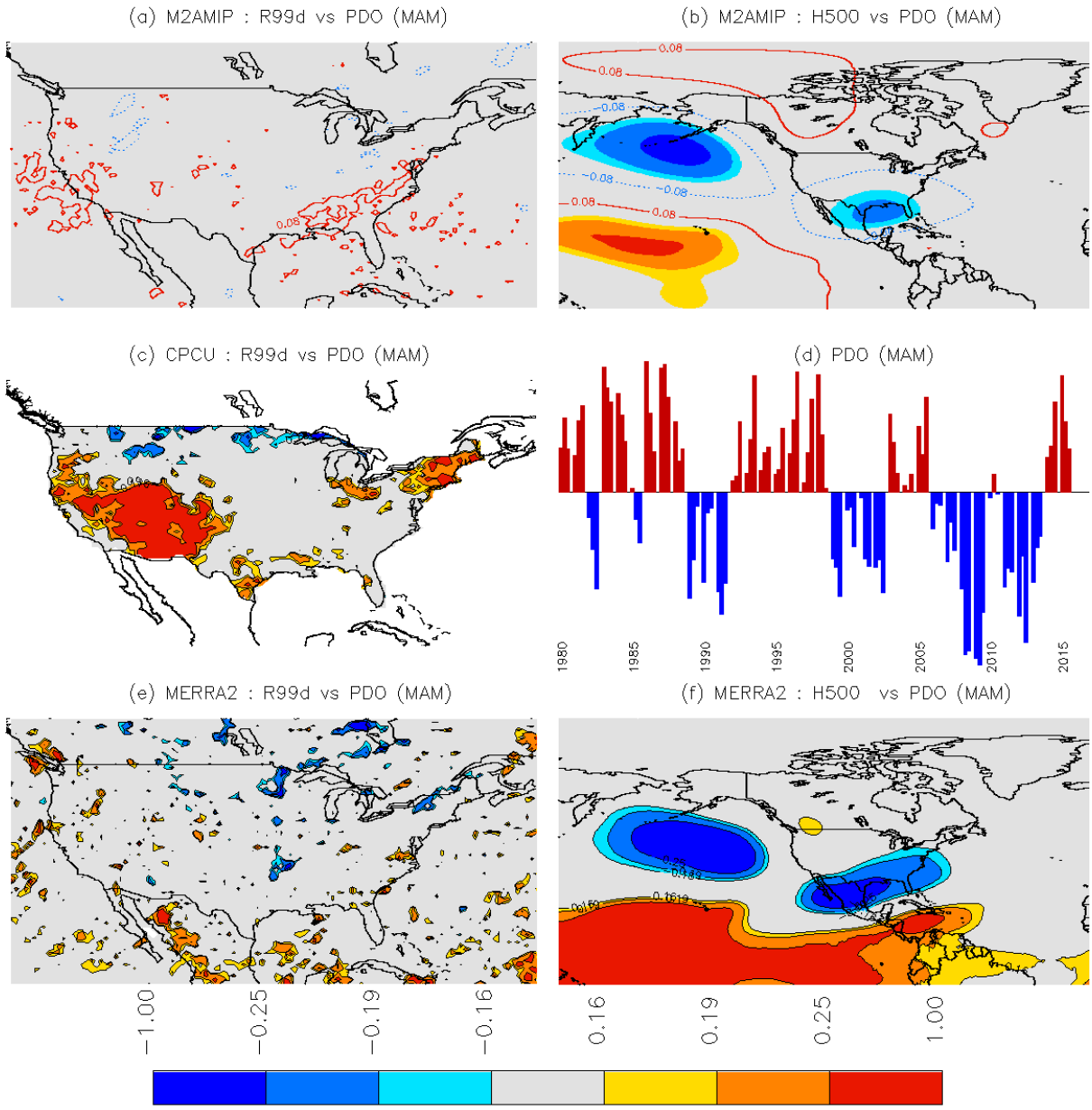

Figure 3.2.3: MAM (a) correlation between PDO index and M2AMIP R99D, (b) correlation between PDO index and 500 hPa heights in M2AMIP, (c) correlation between PDO index and observed R99D, (d) time series of the PDO index, (e) correlation between PDO index and MERRA-2 R99D, and (f) correlation between PDO index and 500 hPa heights in MERRA-2.

The negative correlation between PDO and 500 hPa heights in the southeastern United States during DJF leads to a negative correlation between PDO and mean 2 m temperature in the south and eastern portion of the country, spanning from Texas to New England in MERRA-2, M2AMIP, and the observations. M2AMIP extends this correlation into the Great Plains region for both temperature and 500 hPa heights (Figure 3.2.4). A positive correlation between PDO and 2 m temperature is present in the west. Very similar patterns are seen in the correlations for 90^{th} percentile maximum temperature events (with the same sign) and 10^{th} percentile minimum temperature events (with the opposite sign), in DJF (see supplemental online library), indicating that extreme events are increased along with the mean. The deepening of the Aleutian low during the positive phase of the PDO forces ridging in the west, warming the southwest, and it enhances northerly flow to the east, allowing for cooler air to be advected into southeastern portion of the country (McAfee, 2014). Overall, M2AMIP captures in DJF the observed impact of the PDO on continental US temperatures.

There is good agreement for correlations between temperature and the PDO for the other seasons as well; however, M2AMIP tends to expand the area of significant correlations. The results for TX90P in JJA are a good example of this (Figure 3.2.5). The contour depicting a statistically significant negative correlation for M2AMIP between PDO and 90^{th} percentile temperature events encloses nearly the entire continental United States. On the other hand, neither the observations nor MERRA-2 show a statistically significant negative correlation in regions such as the Northern Great Plains.

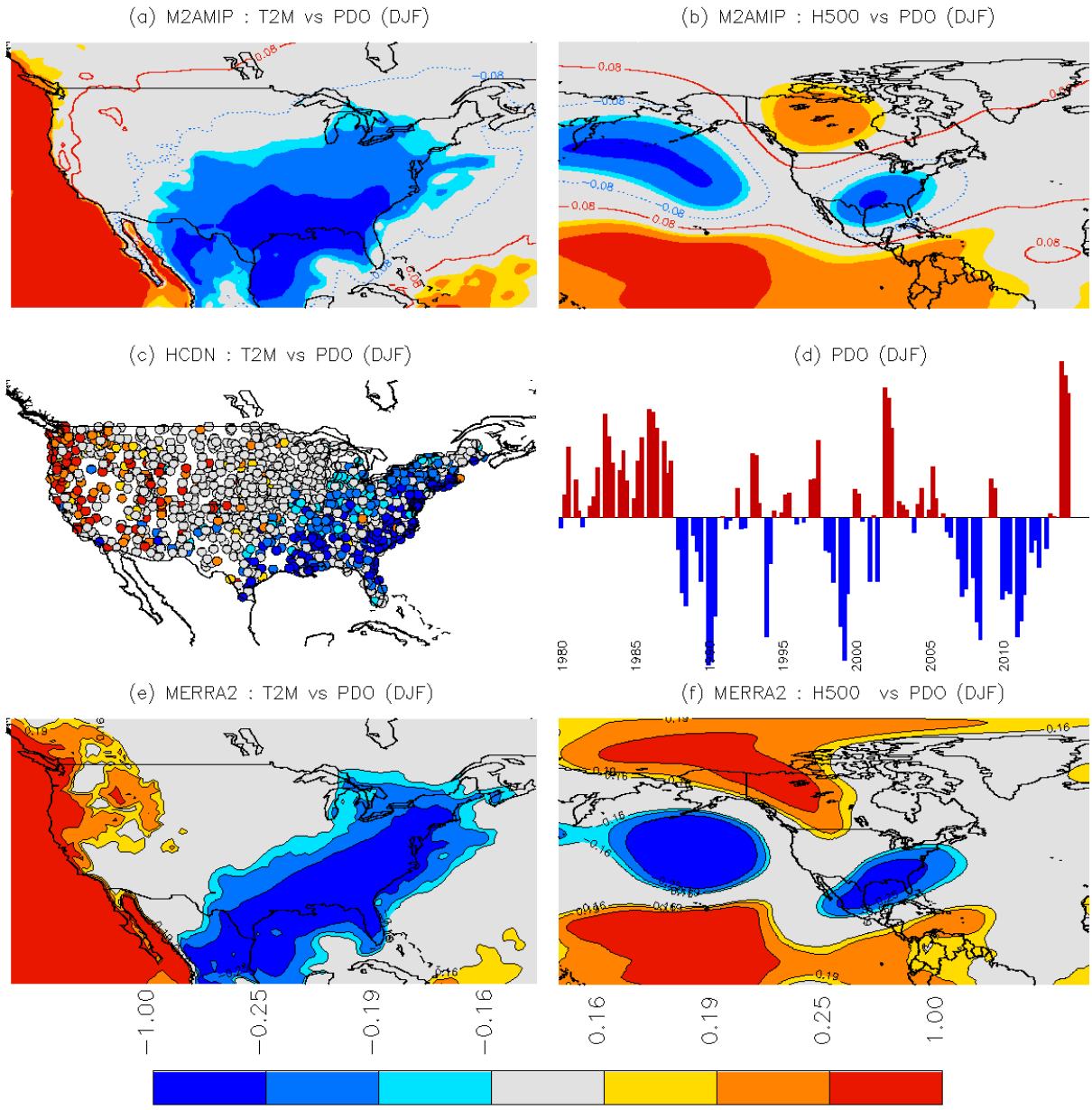

Figure 3.2.4: DJF (a) correlation between PDO index and M2AMIP mean T2M, (b) correlation between PDO index and 500 hPa heights in M2AMIP, (c) correlation between PDO index and observed mean T2M, (d) time series of the PDO index, (e) correlation between PDO index and MERRA-2 mean T2M, and (f) correlation between PDO index and 500 hPa heights in MERRA-2.

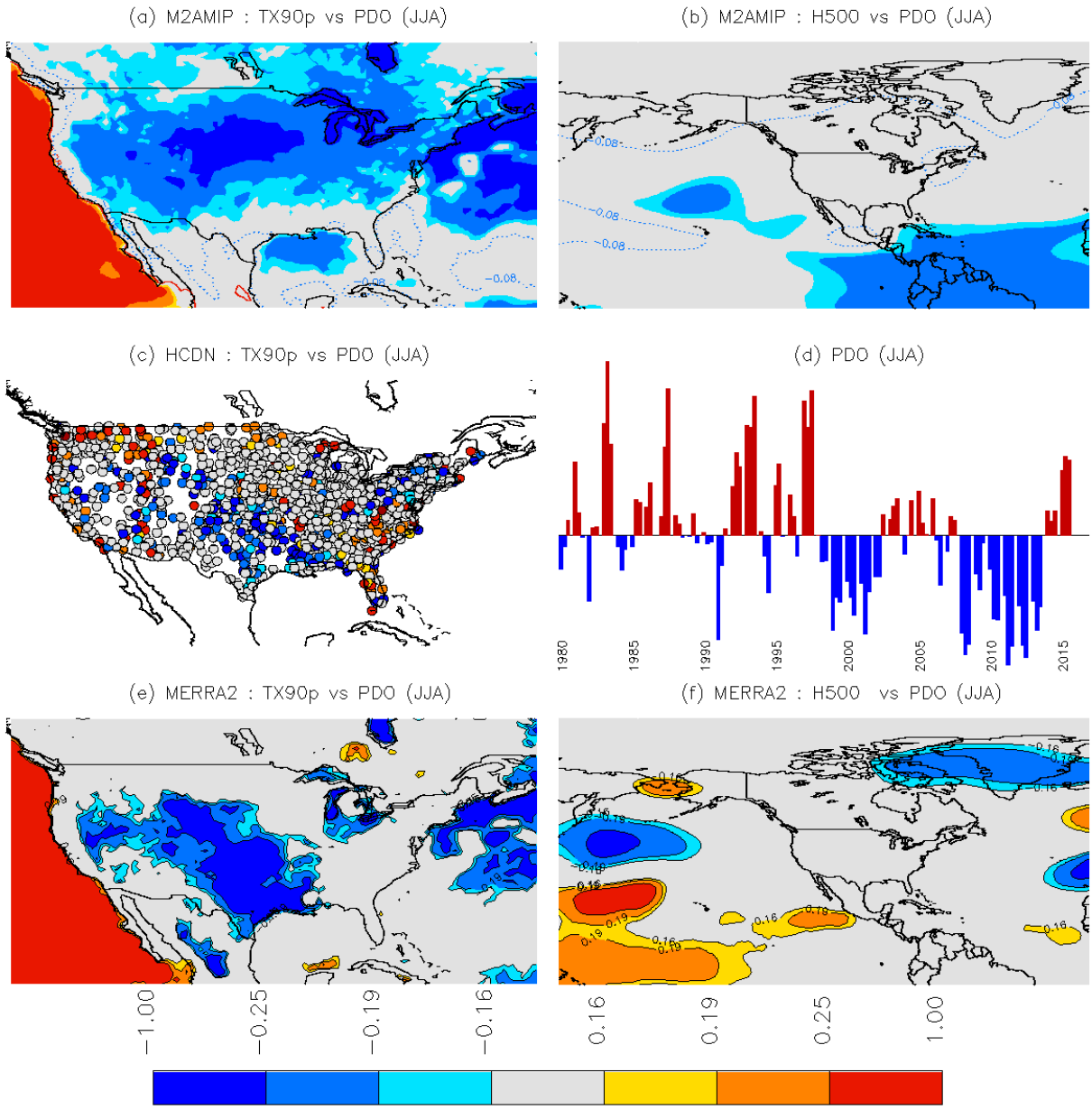

Figure 3.2.5: JJA (a) correlation between PDO index and M2AMIP TX90P, (b) correlation between PDO index and 500 hPa heights in M2AMIP, (c) correlation between PDO index and observed TX90P, (d) time series of the PDO index, (e) correlation between PDO index and MERRA-2 TX90P, and (f) correlation between PDO index and 500 hPa heights in MERRA-2.

3.3 North Atlantic Oscillation

The NAO is characterized by fluctuating dipoles in sea level pressure between the Arctic and subtropical Atlantic Oceans. Anomalies are strongest in the winter and can account for more than one-third of the total variance in sea level pressure over the North Atlantic (Hurrell et al., 2003). As a result, the influence of the NAO during the winter is well documented in the scientific literature, with most studies confined to the winter season (e.g., Wise et al., 2015). The NAO is an important factor for the weather in Europe, but it can also impact the United States, particularly in the eastern part of the country. The positive phase of the NAO is associated with below average sea level pressure in the Arctic and above average sea level pressure to the south, resulting in anomalously southerly flow over the eastern United States and stronger than average surface westerlies across the mid-latitudes of the Atlantic Ocean (Hurrell et al., 2003). There is debate regarding whether the NAO and Arctic Oscillation are two distinct and independent climate features (Ambaum et al., 2001); however, given that their time series are highly correlated (Deser, 2000), we have chosen to analyze only the NAO.

The correlation between DJF total precipitation and the NAO index can be seen in Figure 3.3.1. As a reminder, the NAO index is computed from monthly values, and this is done independently for MERRA-2 and M2AMIP. The observations indicate a negative relationship between the two within an incoherent strip between southern California and North Dakota alongside a positive correlation, smaller in area, to the south (Figure 3.3.1c). The region of the positive correlation is much larger in MERRA-2 and extends to the southwest in MERRA-2 and M2AMIP (Figure 3.3.1a and e). The spatial pattern in the correlation between the NAO index and total precipitation suggests that the NAO is associated with a shift in storm tracks; however, there is no statistically significant difference in storm tracks between high and low NAO years in the United States, though there is over the Atlantic Ocean (Hurrell and Van Loon, 1997). Furthermore, the correlations between the NAO index and precipitation, particularly in the Southwest, are not accompanied by expected correlations between the NAO and 500 hPa heights. The correlations between the NAO index and total precipitation are larger in MERRA-2 than in M2AMIP, although the anomalies in the REOF pattern selected for the NAO are also larger in MERRA-2 (Figure 2.5.1).

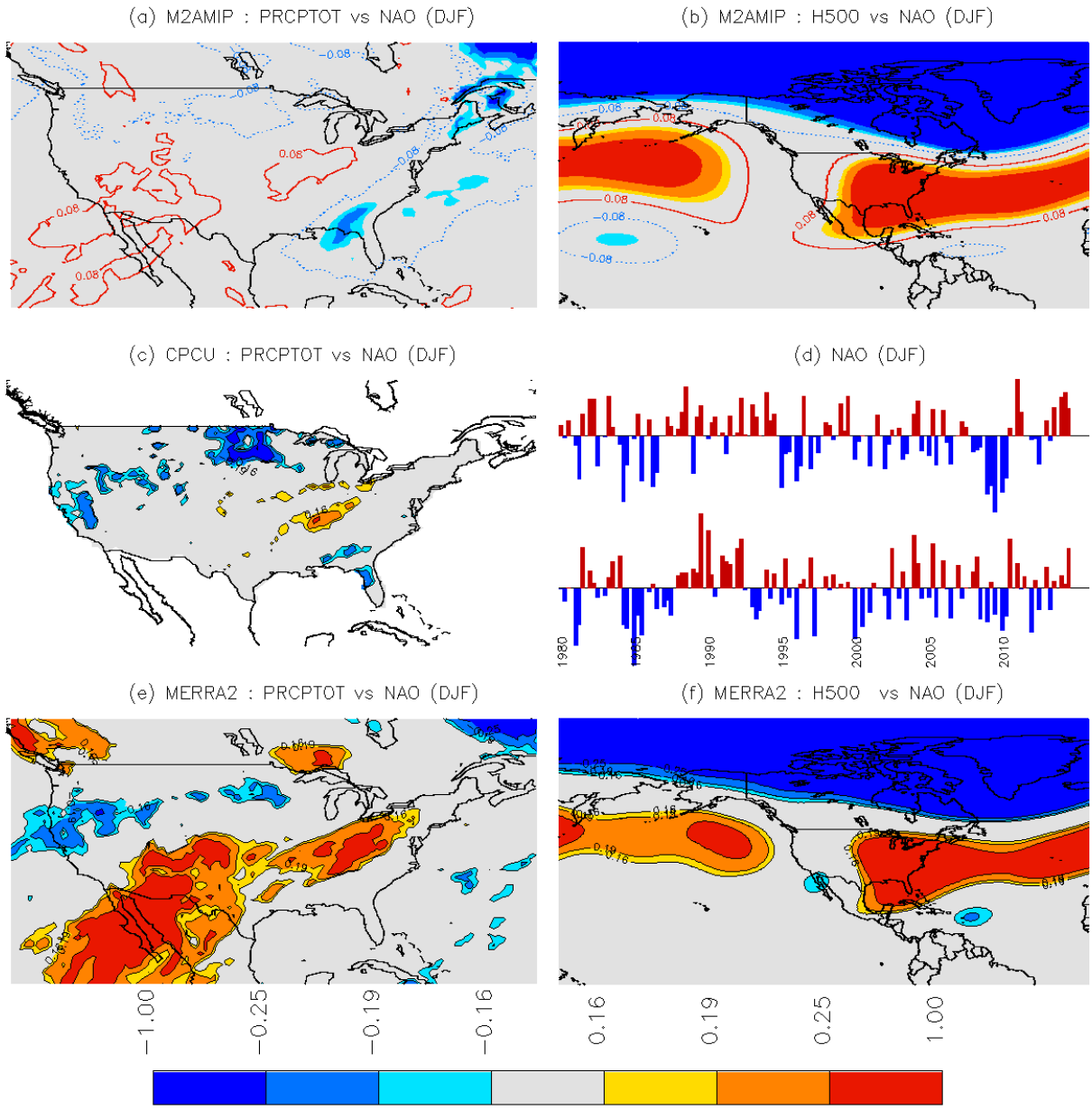

Figure 3.3.1: DJF (a) correlation between NAO index and M2AMIP total precipitation, (b) correlation between NAO index and 500 hPa heights in M2AMIP, (c) correlation between NAO index and observed total precipitation, (d) time series of the NAO index from observations (top) and a representative ensemble member from M2AMIP (bottom), (e) correlation between NAO index and MERRA-2 precipitation, and (f) correlation between NAO index and 500 hPa heights in MERRA-2.

A very similar pattern is seen for extreme precipitation events in the observations, though a lot of scatter is present in MERRA-2 and M2AMIP (see online supplemental library). With respect to the frequency of extreme precipitation events, the observations show negative correlations with the NAO centered in two main areas: the Dakotas and the Ohio River Valley (Figure 3.3.2c). These negative correlations are not present in MERRA-2 or M2AMIP.

The disagreements seen in Figure 3.3.2 are indeed reflected in the literature, with different analyses of observational data suggesting different connections between the NAO and extreme precipitation. Zhang et al. (2010) show that only 6% of observation stations across the United States have a statistically significant difference in extreme precipitation between years with high and low values of the NAO index, with most of the stations exhibiting an influence from the NAO being clustered in the Northeast (Zhang et al., 2010). This is corroborated by Archambault et al. (2008), who state that there is a small increase in extreme precipitation events in the Northeast during the positive phase of the NAO. Ning and Bradley (2015), however, show a negative correlation between the NAO and the intensity and frequency of extreme precipitation events in the Northeast.

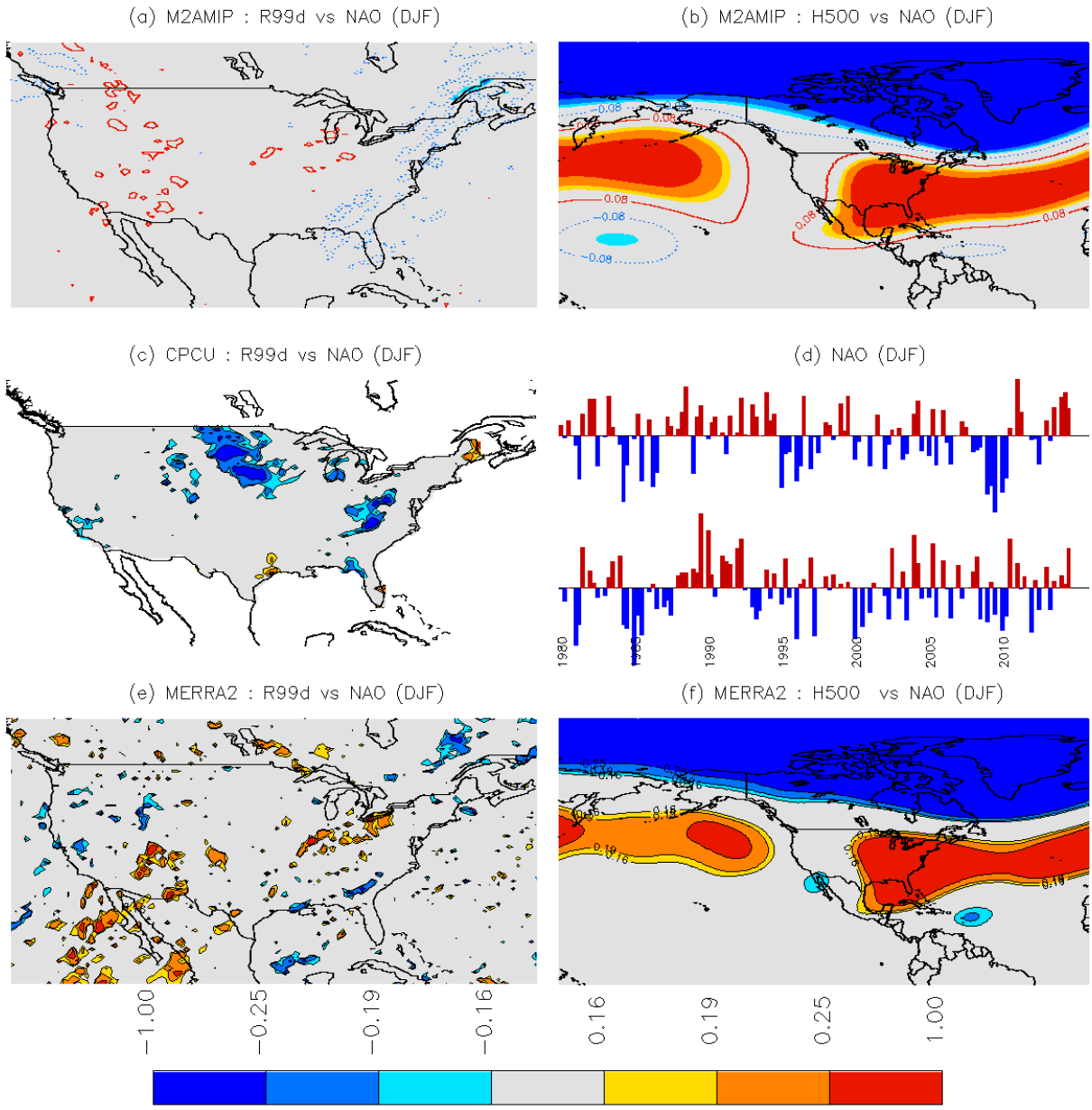

Figure 3.3.2: DJF (a) correlation between NAO index and M2AMIP frequency of 99th percentile precipitation events, (b) correlation between NAO index and 500 hPa heights in M2AMIP, (c) correlation between NAO index and observed frequency of 99th percentile precipitation events, (d) time series of the NAO index from observations (top) and a representative ensemble member from M2AMIP (bottom), (e) correlation between NAO index and MERRA-2 frequency of 99th percentile precipitation events, and (f) correlation between NAO index and 500 hPa heights in MERRA-2.

A much more coherent relationship is present between the NAO and temperature in the US. There is a statistically significant positive correlation between the NAO index and mean 2 m temperature over nearly the entire eastern half of the country in the observations, in MERRA-2, and in M2AMIP, a correlation that is accompanied by a positive correlation in 500 hPa heights (Figure 3.3.3). A stronger counterclockwise flow around the subtropical Atlantic high pressure center is present during the positive phase of the NAO, resulting in southerly winds in the eastern United States (Hurrell et al., 2003).

The pattern for mean 2 m temperature is also largely seen for the temperature extremes. The percentage of time when the maximum temperature exceeds the 90th percentile, for example, also shows positive correlations with the NAO index in the eastern half of the country (Figure 3.3.4a, c, and e). The correlation of the NAO index with the percentage of time the minimum temperature falls below the 10th percentile does show a bit more variability (Figure 3.3.5a, c, and e); still, there is in general a negative correlation in the eastern United States.

As mentioned in the Introduction, despite the intrinsically short time scale of the NAO (less than two weeks), there is considerable evidence that the NAO is modulated by SSTs on much longer time scales. The fact that the two time series of NAO indices shown, e.g., in Fig. 3.3.5d (one based on MERRA-2 and the other based on M2AMIP) appear to have similar long-term variations seems to confirm that this is indeed the case for the time period considered here. In order to better quantify this, we computed the 10-member ensemble mean NAO monthly time series for M2AMIP and correlated it with SST. The results (Figure 3.3.6) indicate that the negative NAO phase occurs more frequently during El Niño events and that the positive NAO phase occurs more frequently during La Niña events.

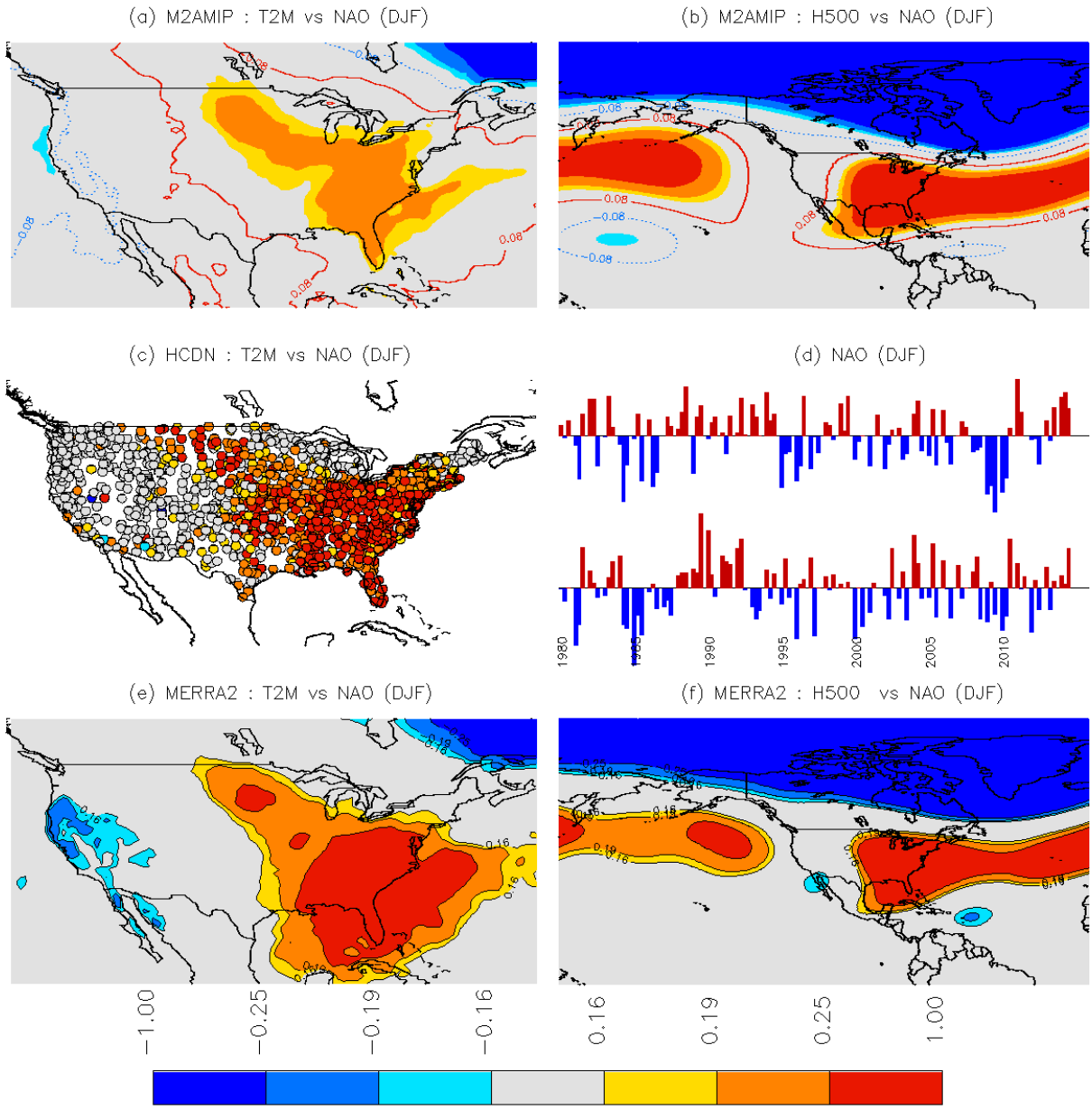

Figure 3.3.3: DJF (a) correlation between NAO index and M2AMIP mean 2 m temperature, (b) correlation between NAO index and 500 hPa heights in M2AMIP, (c) correlation between NAO index and observed mean 2 m temperature, (d) time series of the NAO index from observations (top) and a representative ensemble member from M2AMIP (bottom), (e) correlation between NAO index and MERRA-2 mean 2 m temperature, and (f) correlation between NAO index and 500 hPa heights in MERRA-2.

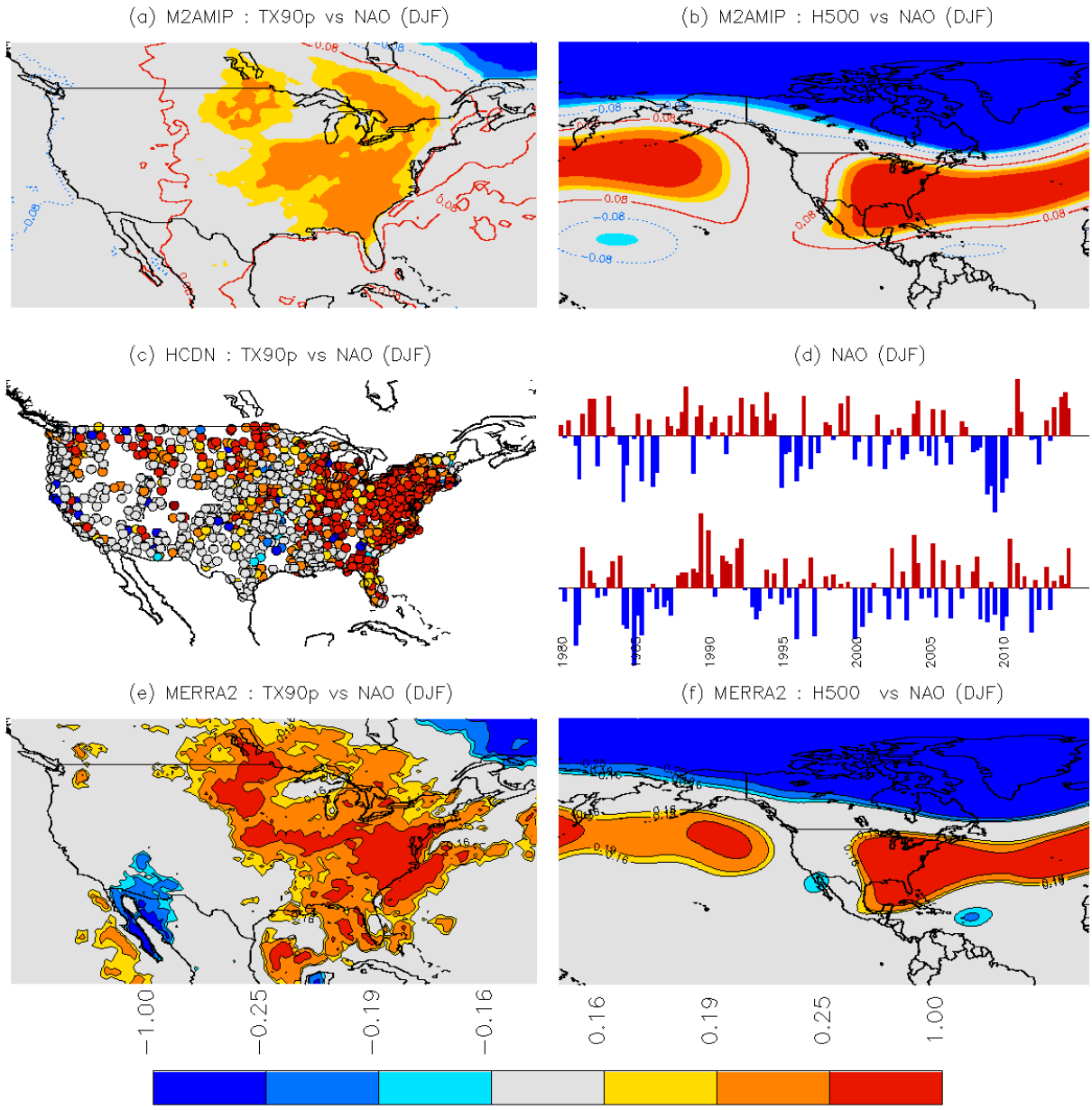

Figure 3.3.4: DJF (a) correlation between NAO index and M2AMIP TX90P, (b) correlation between NAO index and 500 hPa heights in M2AMIP, (c) correlation between NAO index and observed TX90P, (d) time series of the NAO index from observations (top) and a representative ensemble member from M2AMIP (bottom), (e) correlation between NAO index and MERRA-2 TX90P, and (f) correlation between NAO index and 500 hPa heights in MERRA-2.

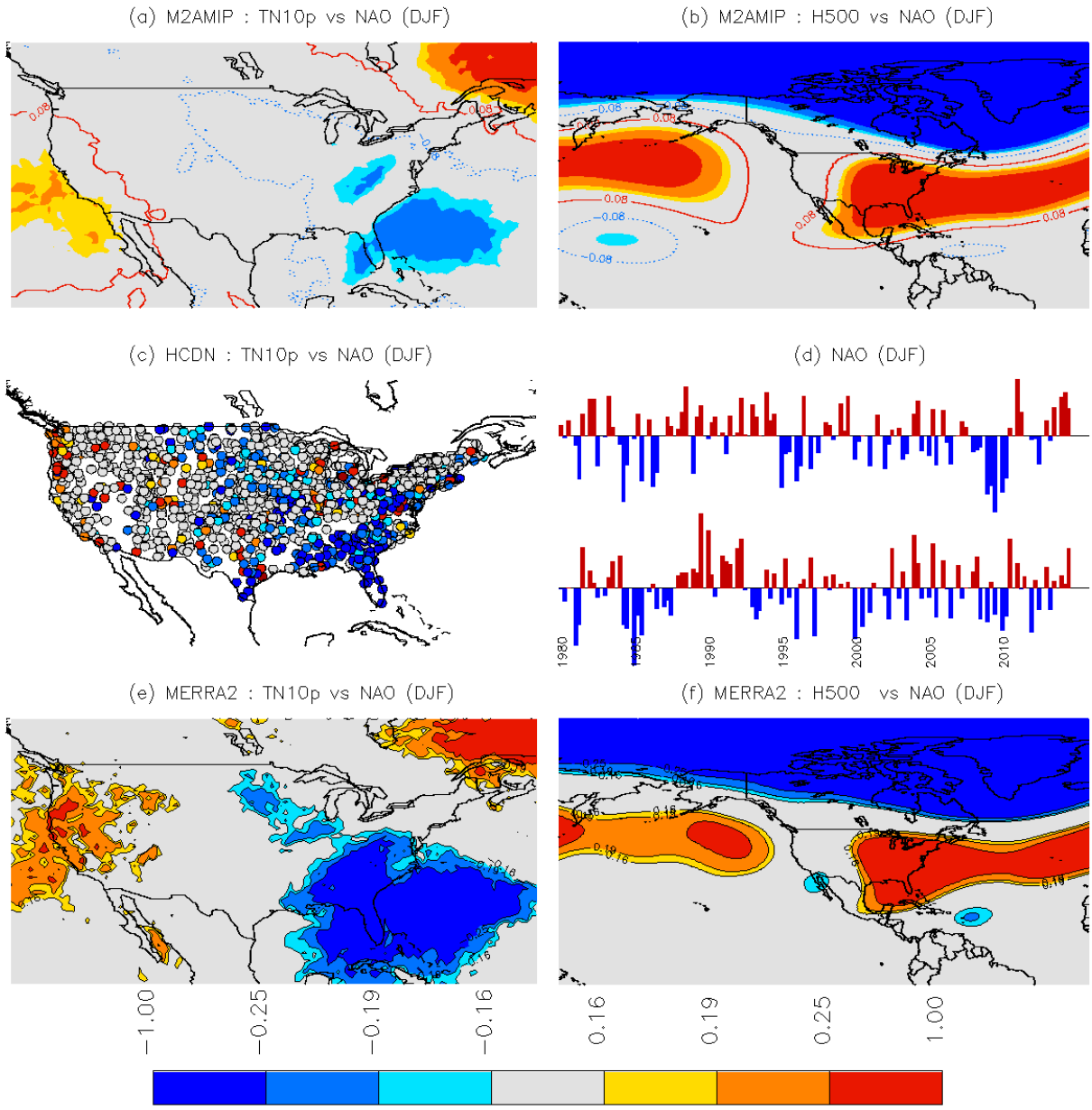

Figure 3.3.5: DJF (a) correlation between NAO index and M2AMIP TN10P, (b) correlation between NAO index and 500 hPa heights in M2AMIP, (c) correlation between NAO index and observed TN10P, (d) time series of the NAO index from observations (top) and a representative ensemble member from M2AMIP (bottom), (e) correlation between NAO index and MERRA-2 TN10P, and (f) correlation between NAO index and 500 hPa heights in MERRA-2.

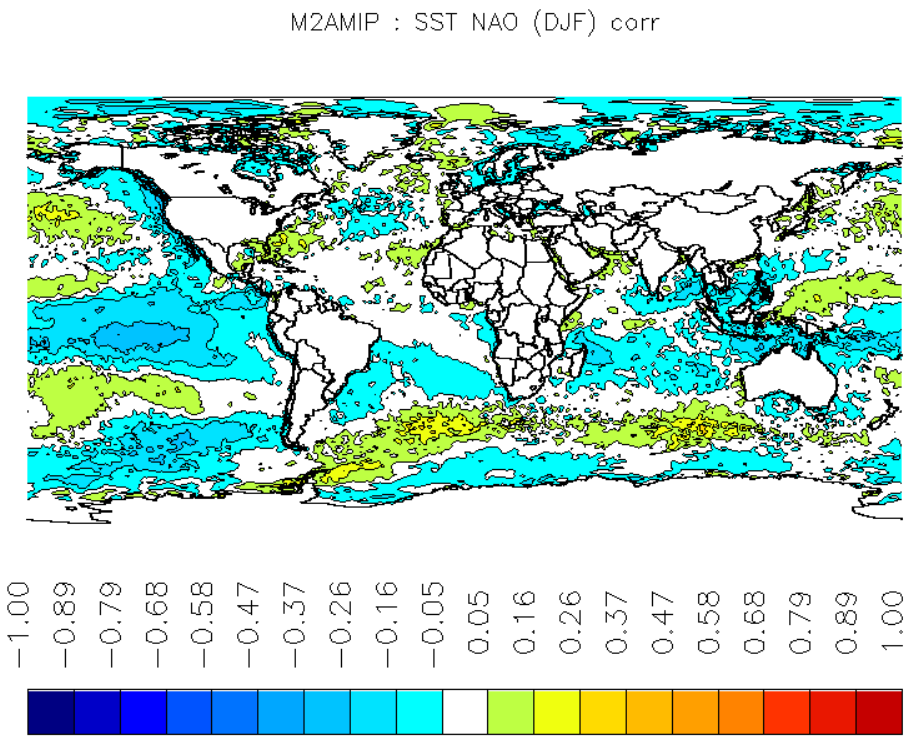

Figure 3.3.6: Correlation between NAO index and SST in M2AMIP during DJF

3.4 Pacific – North American Pattern

The positive phase of the PNA is characterized by ridging, or above-average heights, in the northwestern US and below-average heights associated with a trough in the east (Leathers et al., 1991). This type of pattern results in meridional, as opposed to zonal, flow across the country, which slows the eastward progression of Rossby waves and increases the likelihood of extreme weather events (Francis and Vavrus, 2012). During the negative phase, zonal flow occurs (Leathers et al., 1991).

Correlations between 500 hPa heights and the PNA depict ridging in the west and a trough in the east year round, with the strongest correlations in DJF (Figures 3.4.1b and f) and the weakest correlations in JJA (see online supplemental library). As with the NAO, the correlations here are computed from monthly indices and then averaged over the season. The Northwest US is generally warm and dry in the winter during the positive phase of the PNA; this teleconnection is present in the observations, in MERRA-2, and in M2AMIP (Figures 3.4.1a, c, and e and 3.4.3a, c, and e). The ridge steers storm systems to the north and allows for heat to build up in the area. During the negative phase, storms go through the Northwest, allowing for precipitation, while the enhanced cloud cover lowers the temperature (Leathers et al., 1991). A negative correlation with precipitation is present in the Midwest and Northeast as storms track to the south (Figures 3.4.1a, c, and e). Meanwhile, the Southeast shows a positive correlation for precipitation and a negative correlation for mean 2 m temperature, lying in the trough of the meridional pattern (Figures 3.4.1a, c, and e and 3.4.3a, c, and e). As with the teleconnections previously discussed,

correlation patterns for extreme precipitation characteristics are similar to those for total precipitation, though decreased in magnitude and particularly scattered in MERRA-2 (see online supplemental library). Mallakpour and Villarini (2016b) also show a negative correlation between the PNA and flooding and heavy precipitation events in the Midwest; they concluded that the PNA has a stronger influence on heavy precipitation in the region compared to other teleconnections.

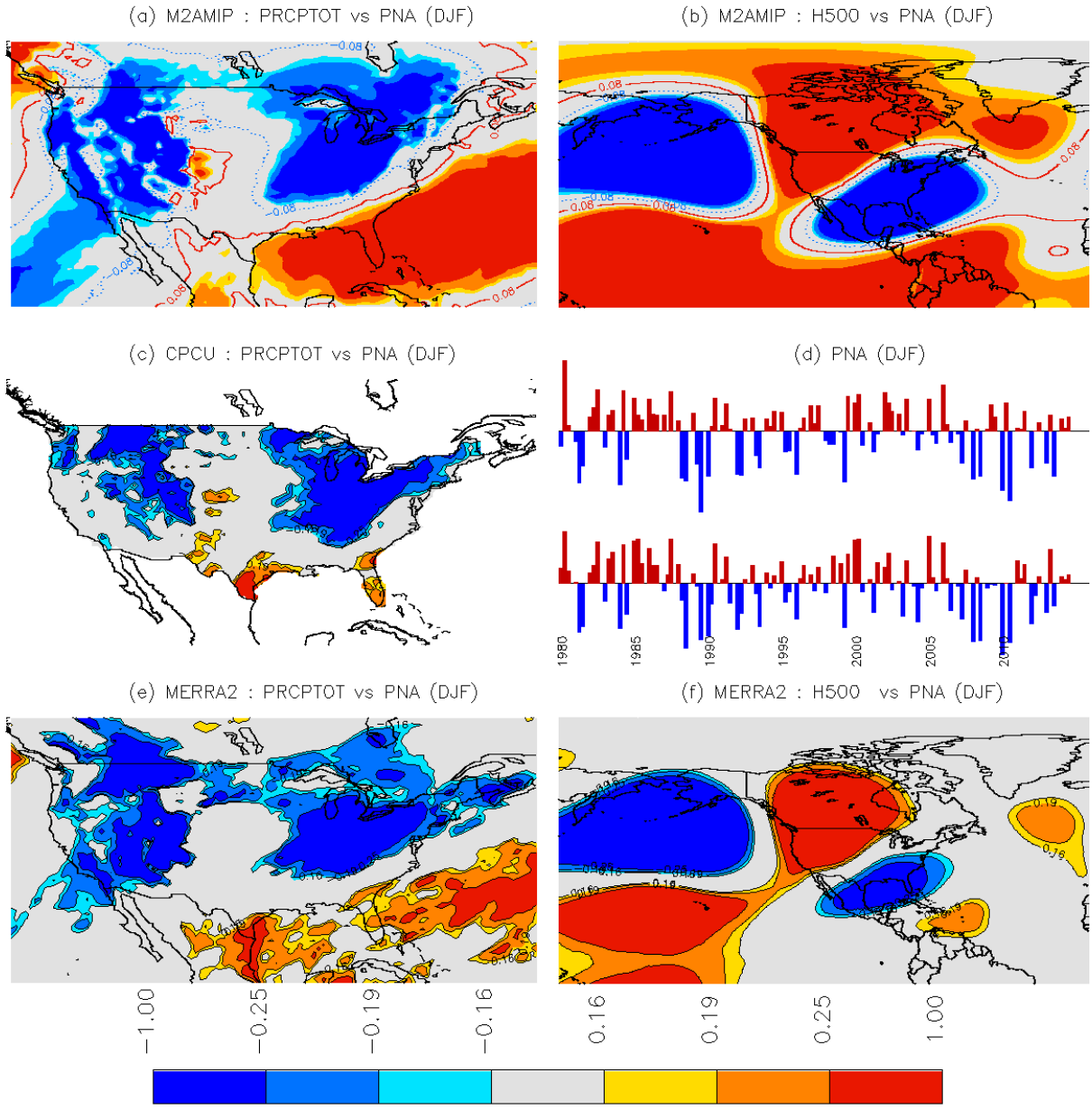

Figure 3.4.1: DJF (a) correlation between PNA index and M2AMIP total precipitation, (b) correlation between PNA index and 500 hPa heights in M2AMIP, (c) correlation between PNA index and observed total precipitation, (d) time series of the PNA index (top) and a representative ensemble member from M2AMIP (bottom), (e) correlation between PNA index

and MERRA-2 precipitation, and (f) correlation between PNA index and 500 hPa heights in MERRA-2.

The above-average 500 mb heights in the Northwest US associated with the PNA result in a positive correlation between the PNA index and mean 2 m temperature extending from southern California to the western edge of the Great Lakes – a feature that is found in the observations and MERRA-2 and is successfully reproduced in M2AMIP (Figure 3.4.2a, c, and e). The other half of the country shows a negative correlation as the positive phase of the PNA enables cold air from Canada to be advected towards the southeast. Overall, the correlation pattern across the country for 2 m temperature is very similar to the pattern for 500 mb height. Warmer mean temperatures in the Northwest decrease the likelihood of a minimum temperature below the 10^{th} percentile (Figure 3.4.3a, c, and e); however, the relationship between the PNA and cold air outbreaks in the eastern portion of the country is not as straightforward. Observations indicate a positive correlation between the PNA and TN10P in Georgia and, to a lesser extent, in the Mid-Atlantic region, but MERRA-2 does not exhibit a positive statistically significant relationship anywhere in the country (Figure 3.4.5c and e). On the other hand, M2AMIP has a statistically significant positive correlation between PNA and TN10P from Texas through southern Maine (Figure 3.4.3a). Westby et al. (2013) shows a positive correlation between the PNA and cold air outbreaks along the entire east coast, and extending westward into Texas, very similar to what is present in M2AMIP, though the relationship presented in that study is not statistically significant outside the southern tip of Florida. Ning and Bradley (2015) also show a positive correlation between PNA and cold days and nights in the northeastern United States, but they do not address statistical significance. From a different perspective, Loikith and Broccoli (2014) showed that over 30% of days in DJF that meet the criteria for TN10P occur while the PNA is in the positive phase.

As is the case for the NAO, the PNA (despite having relatively short intrinsic time scales) appears to be modulated by SST on seasonal and longer time scales, as is evident from the two time series shown, for example, in Figure 3.4.3d. Here again we have computed the ensemble mean of the 10-member ensemble of PNA indices and then correlated that with SST. The correlations (in the online supplemental library) show a clear link of the ensemble mean PNA index to ENSO, with El Nino (La Nina)-like SST anomalies in the tropical Pacific associated with the positive (negative) phase of the PNA. The ensemble mean time series also shows a decadal-scale change with a shift toward more negative values after the late 1990s – the time at which the PDO underwent a shift to the negative phase as well. In fact, the SST correlation pattern has some PDO characteristics in the North Pacific, which suggests that the PNA is also modulated by PDO-related SST variations. It is, however, unclear whether these correlations represent a true modulation of the PNA index by SST or whether they simply represent a projection of the ENSO (or PDO) response on the PNA pattern, an issue that is still debated in the literature and beyond the scope of this report.

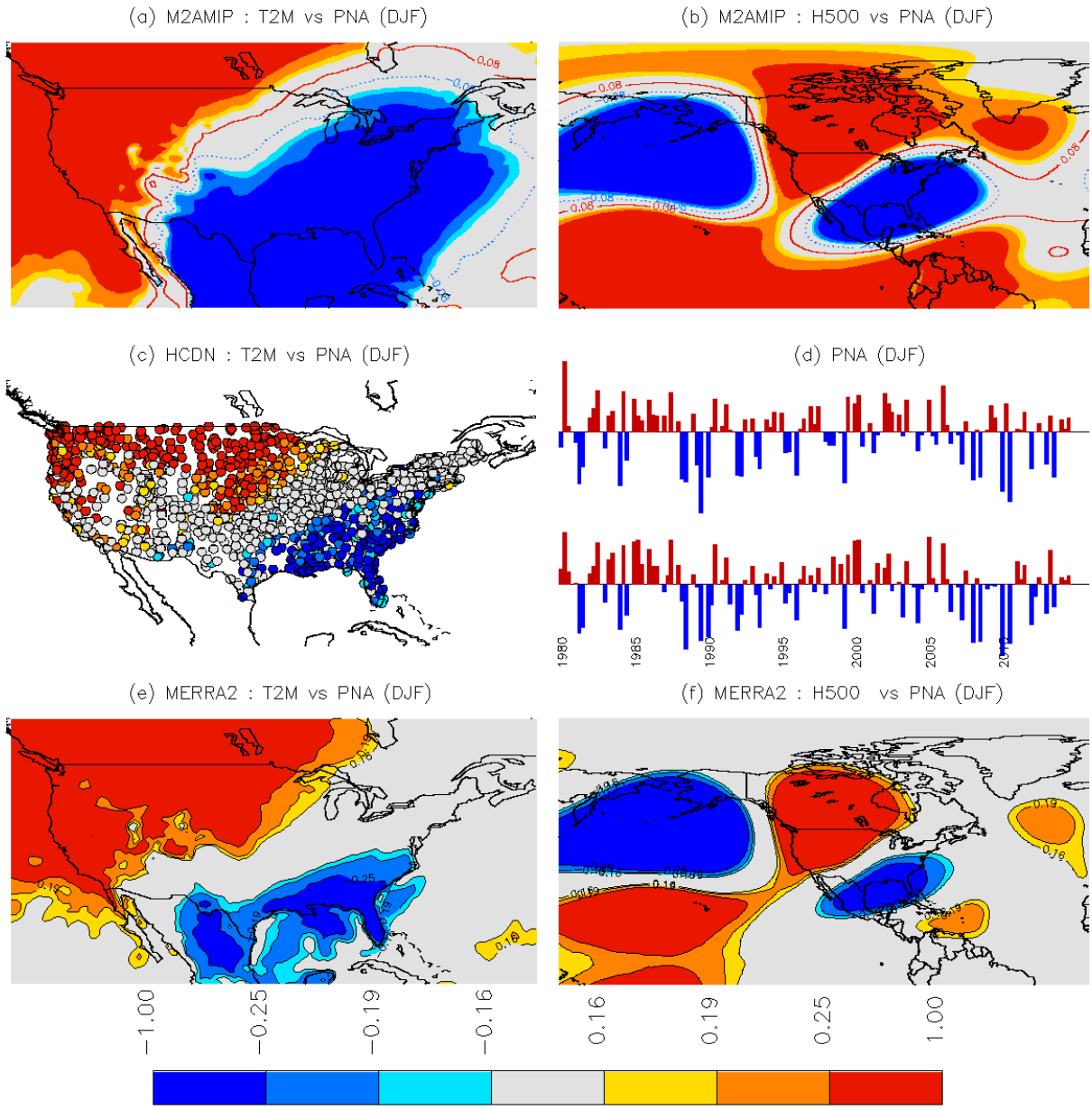

Figure 3.4.2: DJF (a) correlation between PNA index and M2AMIP daily mean 2 m temperature, (b) correlation between PNA index and 500 hPa heights in M2AMIP, (c) correlation between PNA index and observed daily mean 2 m temperature, (d) time series of the PNA index from observations (top) and a representative ensemble member from M2AMIP (bottom), (e) correlation between PNA index and MERRA-2 daily mean 2 m temperature, and (f) correlation between PNA index and 500 hPa heights in MERRA-2.

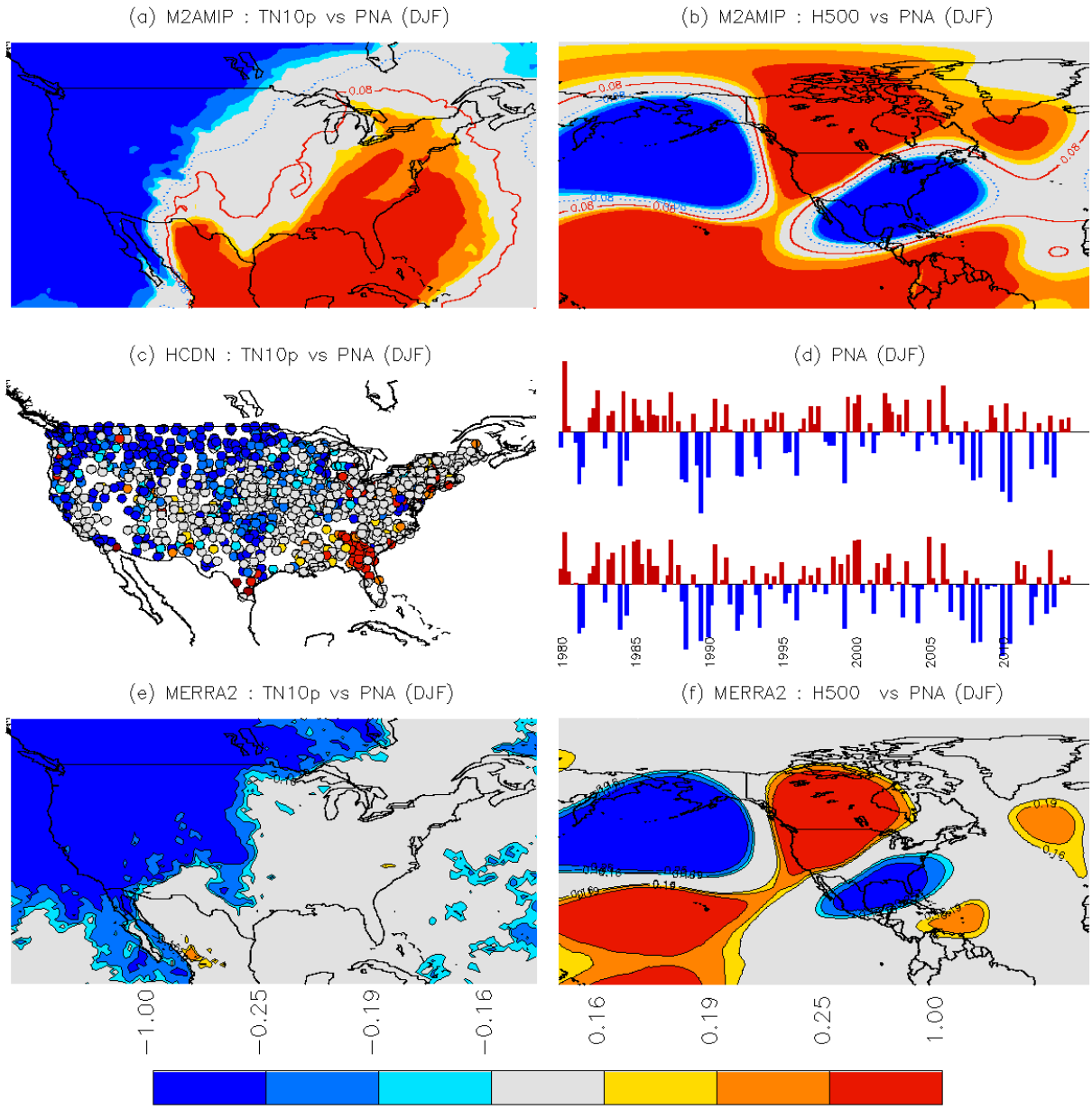

Figure 3.4.3: DJF (a) correlation between PNA index and M2AMIP daily minimum 2 m temperature, (b) correlation between PNA index and 500 hPa heights in M2AMIP, (c) correlation between PNA index and observed daily minimum 2 m temperature, (d) time series of the PNA index from observations (top) and a representative ensemble member from M2AMIP (bottom), (e) correlation between PNA index and MERRA-2 daily minimum 2 m temperature, and (f) correlation between PNA index and 500 hPa heights in MERRA-2.

4. Summary

The response of daily mean and extreme temperature and precipitation over the US to teleconnection patterns was evaluated in version 5.12.4 of the Goddard Earth Observing System by analyzing associated seasonal correlations in MERRA-2, in an ensemble of AMIP-type simulations, and in observations. The M2AMIP simulations in particular represent the behavior of the free running model; our analyses herein largely focus on whether this free running model captures the observed teleconnections. Four well-documented atmospheric teleconnection patterns in particular, related to ENSO, PDO, NAO, and PNA, were examined, with discussion herein centered on the subset of the correlation maps with noteworthy features. All figures from the analysis, however, can be found in the supplemental online library; also, Appendix A below provides tables showing the fraction of area with statistically significant relationships.

Regardless of the teleconnection pattern, the largest correlations and agreement between the model and observations tended to be during DJF. While there was generally good agreement between M2AMIP and the observations, there is room for improvement in the model. In situations where M2AMIP was able to capture the correlations from the observations, M2AMIP overextended the area of statistically significant correlations, as is also apparent from the tables in Appendix A. At times M2AMIP demonstrates a relationship that is not present in the observations, as was the case for mean and extreme temperature in relation to the PDO during JJA, extreme cold events in relation to Niño3.4 in DJF, and mean precipitation in the Southwest in relation to the NAO during DJF. There were also cases, mostly confined to frequency of extreme precipitation events, for which neither M2AMIP nor MERRA-2 agreed with the observations. Significant correlations for extreme precipitation events tended to be very scattered in MERRA-2 and M2AMIP but coherent in the observations. A possible contributing factor to this could be discrepancies in the number of days with precipitation going into the calculation of the number of days exceeding the 90^{th}, 95^{th}, or 99^{th} percentiles.

Two important topics that have not been discussed here are the interactions of teleconnections and the nonlinearity of responses to teleconnections. Multiple teleconnection patterns can be present at the same time, a topic of numerous studies (eg. Archambault et al., 2008; Lim and Schubert, 2011; Wise et al., 2015; Fuentes-Franco et al., 2016). Lim and Schubert (2011) demonstrate the negative height anomaly in the southeastern United States associated with the Arctic Oscillation can interrupt the development of a positive height anomaly associated with La Niña. The impact of the positive phase of ENSO can also be stronger during the positive phase of the PDO (Fuentes-Franco et al., 2016). Examining this latter interaction with the observations and MERRA-2 data is difficult given the limited number of samples with particular ENSO and PDO phase combinations, but such an analysis is possible with the ten member M2AMIP ensemble. Figure 4.1 shows the anomaly in 2 m temperature, for DJF, during different combinations of the phases of ENSO and the PDO in the M2AMIP results. The spatial pattern in the anomaly when both the ENSO and PDO are in the positive is very similar to the spatial pattern seen in the correlation. However, there are some subtle differences, which also speak to the nonlinearity of teleconnections; for example, the area of the negative anomaly in the Southeast when both phases are positive does not extend as far north and west as the positive anomaly when both phases are negative, which is actually more similar to the negative correlations between 2 m temperature and the PDO or ENSO seen in section 3. Zhang et al.

(2016) noticed an asymmetry in the response to the positive and negative phases of ENSO in AMIP simulations as well.

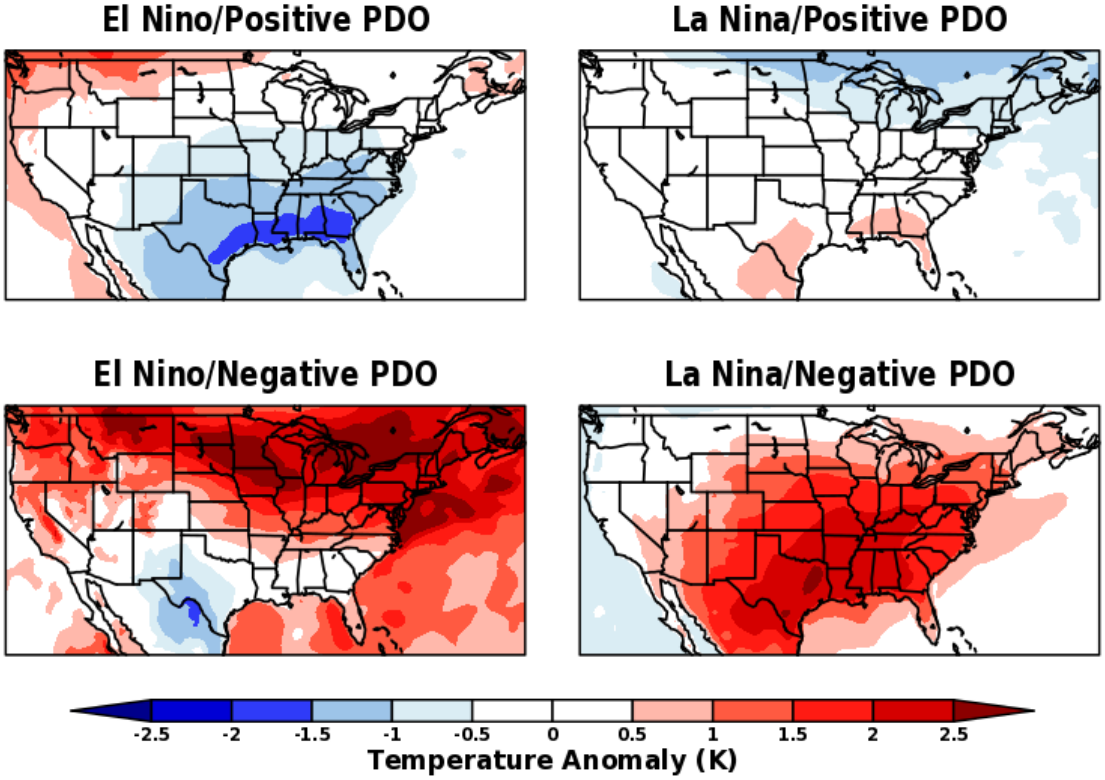

Figure 4.1: The anomaly in 2 m temperature with respect to climatology during (top left) the positive phase of ENSO and PDO, (top right) the negative phase of ENSO and the positive phase of the PDO, (bottom left) the positive phase of ENSO and the negative phase of the PDO, and (bottom right) the negative phase of ENSO and the PDO.

5. References

Alexander L. V., 2015: Global observed long-term changes in temperature and precipitation extremes: A review of progress and limitations in IPCC assessments and beyond. Weather and Climate Extremes, 11, 4-6, doi:10.1016/j.wace.2015.10.007.

Ambaum, M., B. Hoskins, and D. Stephenson, 2001: Arctic Oscillation or North Atlantic Oscillation?. J. Climate, 14, 3495–3507, doi: 10.1175/1520-0442(2001)014<3495:AOONAO>2.0.CO;2.

Archambault, H., L. Bosart, D. Keyser, and A. Aiyyer, 2008: Influence of Large-Scale Flow Regimes on Cool-Season Precipitation in the Northeastern United States. Mon. Wea. Rev., 136, 2945–2963, doi: 10.1175/2007MWR2308.1.

Barlow, M., S. Nigam, and E. H. Berbery, 2001: ENSO, Pacific Decadal Variability, and U.S. Summertime Precipitation, Drought, and Stream Flow. J. Climate, 14, 2105–2128, doi: 10.1175/1520-0442(2001)014<2105:EPDVAU>2.0.CO;2.

Barnston, A. and R. Livezey, 1987: Classification, Seasonality and Persistence of Low-Frequency Atmospheric Circulation Patterns. Mon. Wea. Rev., 115, 1083–1126, doi: 10.1175/1520-0493(1987)115<1083:CSAPOL>2.0.CO;2.

Bjerknes, J., 1969: Atmospheric teleconnections from the equatorial Pacific. Monthly Weather Review, 97, 163-172.

Bosilovich, M. G., 2013: Regional Climate and Variability of NASA MERRA and Recent Reanalyses: U.S. Summertime Precipitation and Temperature. J. Appl. Meteor. Climatol., 52, 1939–1951, doi: 10.1175/JAMC-D-12-0291.1.

Bosilovich, M. G., et al., 2015: MERRA-2: Initial Evaluation of the Climate. NASA/TM–2015–104606, Vol. 43, 139 pp.

Chen, M., and P. Xie, 2008: CPC Unified Gauge-Based Analysis of Global Daily Precipitation. Western Pacific Geophysics Meeting, Cairns, Australia, Amer. Geophys.Union, Abstract A24A-05.

Deser, C., 2000: On the teleconnectivity of the “Arctic Oscillation” .Geophys. Res. Lett., 27, 779–782, doi:10.1029/1999GL010945.

Donlon, C. J., M. Martin, J. Stark, J. Roberts-Jones, E. Fiedler, and W. Wimmer, 2012: TheOperational Sea Surface Temperature and Sea Ice Analysis (OSTIA) system. RemoteSens. Environ., 116, 140–158, doi:10.1016/j.rse.2010.10.017.

Dourte, D. R., E. Gelcer, O.Uryasev, C. G.Staub, D. D.Barreto, and C. W. Fraisse, 2016: Gridded, monthly rainfall and temperature climatology for El Niño Southern Oscillation impacts in the United States. Int. J. Climatol.,doi:10.1002/joc.4820.

Feldstein, S. B., 2000: The timescale, power spectra, and climate noise properties of teleconnection patterns. *J. Climate*, **13,** 4430–4440.

Francis, J. A., and S. J. Vavrus, 2012: Evidence linking Arctic amplification to extreme weather in mid-latitudes, Geophys. Res. Lett., 39, L06801, doi:10.1029/2012GL051000.

Fuentes-Franco, R., F. Giorgi, E. Coppola, and F. Kucharski, 2016: The role of ENSO and PDO in variability of winter precipitation over North America from twenty first century CMIP5 projections.ClimDyn, 46, 3259-3277, doi:10.1007/s00382-015-2767-y.

Gates, W. L.,1992: AMIP: The Atmospheric Model Intercomparison Project. *Bull. Ameri. Meteor. Soc.*, **73**, 1962-1970.

Gelaro, R. et al., 2017: The Modern-Era Retrospective Analysis for Research and Applications, Version 2 (MERRA-2), J. Climate, accepted.

Global Modeling and Assimilation Office (GMAO), 2015a: MERRA-2 statD_2d_slv_Nx: 2d,Daily,Aggregated Statistics,Single-Level,Assimilation,Single-Level Diagnostics V5.12.4, Greenbelt, MD, USA, Goddard Earth Sciences Data and Information Services Center (GES DISC), doi:10.5067/9SC1VNTWGWV3.

Global Modeling and Assimilation Office (GMAO), 2015b: MERRA-2 tavg1_2d_flx_Nx: 2d,1-Hourly,Time-Averaged,Single-Level,Assimilation,Surface Flux Diagnostics V5.12.4, Greenbelt, MD, USA, Goddard Earth Sciences Data and Information Services Center (GES DISC), doi:10.5067/7MCPBJ41Y0K6.

Global Modeling and Assimilation Office (GMAO), 2015c: MERRA-2 tavgM_2d_slv_Nx: 2d,Monthly mean,Time-Averaged,Single-Level,Assimilation,Single-Level Diagnostics V5.12.4, Greenbelt, MD, USA, Goddard Earth Sciences Data and Information Services Center (GES DISC), doi:10.5067/AP1B0BA5PD2K.

Goddard, L., S. J. Mason, S.E.Zebiak, C. F.Ropelewski, R. Basher, and M. A. Cane, 2001: Current approaches to seasonal to interannual climate predictions. Int. J. Climatol., 21, 1111–1152, doi:10.1002/joc.636.

Hoell, A., C. Funk, C. and M. Barlow, 2014: The regional forcing of Northern hemisphere drought during recent warm tropical west Pacific Ocean La Niña events. Clim. Dyn., 42, 3289-3311, doi:10.1007/s00382-013-1799-4.

Hoell, A., M. Hoerling, J. Eischeid, K. Wolter, R. Dole, J.Perlwitz, T. Xu, and L. Cheng, 2016: Does El Niño intensity matter for California precipitation?.Geophys. Res. Lett., 43, 819–825, doi:10.1002/2015GL067102.

Hurrell, J. W., and H. van Loon, 1997: Decadal variations in climate associated with the North Atlantic Oscillation, Climatic Change, 36,301–326, doi: 10.1023/A:1005314315270.

Hurrell, J. W., Y. Kushnir, G.Ottersen, and M. Visbeck, 2003: An Overview of the North Atlantic Oscillation, in The North Atlantic Oscillation: Climatic Significance and Environmental Impact, American Geophysical Union, Washington, D. C..doi: 10.1029/134GM01.

Katz, R. W., 2002: Sir Gilbert Walker and a connection between El Niño and Statistics. Statistical Science, 17, 97-112, doi:10.1214/ss/1023799000.

Leathers, D. J., B.Yarnal, M. A. Palecki, 1991: The Pacific/North American Teleconnection Pattern and United States Climate. Part I: Regional Temperature and Precipitation Associations. J. Climate, 4, 517–528, doi: 10.1175/1520-0442(1991)004<0517:TPATPA>2.0.CO;2.

Lim, Y. and K. Kim, 2007: ENSO Impact on the Space–Time Evolution of the Regional Asian Summer Monsoons. J. Climate, 20, 2397–2415, doi: 10.1175/JCLI4120.1.

Lim, Y.-K., and S. D. Schubert , 2011: The impact of ENSO and the Arctic Oscillation on winter temperature extremes in the southeast United States. Geophys. Res. Lett., 38, L15706, doi:10.1029/2011GL048283.

Loikith, P. and A. Broccoli, 2014: The Influence of Recurrent Modes of Climate Variability on the Occurrence of Winter and Summer Extreme Temperatures over North America. J. Climate, 27, 1600–1618, doi: 10.1175/JCLI-D-13-00068.1.

McAfee, S., 2014: Consistency and the Lack Thereof in Pacific Decadal Oscillation Impacts on North American Winter Climate. J. Climate, 27, 7410–7431, doi: 10.1175/JCLI-D-14-00143.1.

Mallakpour, I. and G. Villarini, 2016a:Analysis of changes in the magnitude, frequency, and seasonality of heavy precipitation over the contiguous USA.Theor Appl. Climatol.,doi:10.1007/s00704-016-1881-z.

Mallakpour, I. and G. Villarini, 2016b: Investigating the relationship between the frequency of flooding over the central United States and large-scale climate. Advances in Water Resources, 92, 159-171, doi: 10.1016/j.advwatres.2016.04.008.

Mantua, N.J. and S.R. Hare, Y. Zhang, J.M. Wallace, and R.C. Francis,1997: A Pacific interdecadal climate oscillation with impacts on salmon production. Bulletin of the American Meteorological Society, 78, pp. 1069-1079.

Mantua, N. J. and S. R. Hare, 2002: The Pacific Decadal Oscillation. Journal of Oceanography, 58, 35-44, doi: 10.1023/A:1015820616384.

McCarty, W. et al., 2016: MERRA-2 Input Observations: Summary and Assessment. NASA Technical Report Series on Global Modeling and Data Assimilation, NASA/TM-2016-104606, Vol. 46, 61 pp

Menne, M.J., I. Durre, R.S. Vose, B.E. Gleason, and T.G. Houston, 2012: An overview of the Global Historical Climatology Network-Daily Database. Journal of Atmospheric and Oceanic Technology, 29, 897-910, doi:10.1175/JTECH-D-11-00103.1.

Molod, A., L. Takacs, M. Suarez, and J. Backmeister, 2015: Development of the GEOS-5 atmospheric general circulation model: evolution from MERRA to MERRA2. *Geosci. Model Dev.*, **8**, 1339-1356, doi: 10.5194/gmd-8-1339-2015.

Mosedale, T. J., D. B. Stephenson, M. Collins, and T. C. Millsu, 2006: Granger causality of coupled climate processes: Ocean feedback on the North Atlantic Oscillation. J. Climate, 19, 1182–1194.

Newman, M., M. Alexander, T. Ault, K. Cobb, C. Deser, E. Di Lorenzo, N. Mantua, A. Miller, S. Minobe, H. Nakamura, N. Schneider, D. Vimont, A. Phillips, J. Scott, and C. Smith, 2016: The Pacific Decadal Oscillation, Revisited. *J. Climate,* **29**, 4399–4427, doi: 10.1175/JCLI-D-15-0508.1.

Ning, L. and R. Bradley, 2015: Winter Climate Extremes over the Northeastern United States and Southeastern Canada and Teleconnections with Large-Scale Modes of Climate Variability. J. Climate, 28, 2475–2493, doi: 10.1175/JCLI-D-13-00750.1.

Randles, C. A., A. da Silva, V. Buchard, P. R. Colarco, A. S. Darmenov, R. C. Govindaraju, A. Smirnov, R. A. Ferrare, J. W. Hair, Y. Shinozuka, and C. Flynn, 2017: The MERRA-2 Aerosol Reanalysis, 1980-onward, Part I: System Description and Data Assimilation Evaluation. J. Climate.

Reichle, R., Q. Liu, R. Koster, C. Draper, S. Mahanama, and G. Partyka, 2017: Land Surface Precipitation in MERRA-2. J. Climate, 30, 1643–1664, doi: 10.1175/JCLI-D-16-0570.1.

Reynolds, R. W., T. M. Smith, C. Liu, D. B. Chelton, K. S. Casey, and M. G. Schlax, 2007:Daily high-resolution-blended analyses for Sea Surface Temperature. J. Climate, 20, 5473–5496, doi:10.1175/2007JCLI1824.1.

Rienecker, M.M., M. J. Suarez, R. Todling, J. Bacmeister, L. Takacs, H.-C. Liu, W. Gu, M. Sienkiewicz, R. D. Koster, R. Gelaro, I. Stajner, and J. E. Nielsen, 2008: The GEOS-5 Data Assimilation System - Documentation of Versions 5.0.1, 5.1.0, and 5.2.0. Technical Report Series on Global Modeling and Data Assimilation, Vol. 27, 1-118 pp.

Schubert, S., and Coauthors, 2009: A US CLIVAR Project to Assess and Compare the Responses of Global Climate Models to Drought-Related SST Forcing Patterns: Overview and Results. J. Climate, 22, 5251-5272.

Schubert, S. D., and Y.-K. Lim, 2013: Climate variability and weather extremes: model simulated and historical data. Chapter 9 in a book entitled "Extremes in a changing climate: Detection, analysis, and uncertainty" by Sorooshian et. al. editors., Water Science and Technology Library 65, doi:10.1007/978-94-007-4479-0_9, Springer, 239-285.

Seager, R., M. Hoerling, S. Schubert, H. Wang, B. Lyon, A. Kumar, J. Nakamura, and N. Henderson, 2015: Causes of the 2011–14 California Drought. *J. Climate,* **28**, 6997–7024, doi: 10.1175/JCLI-D-14-00860.1.

Straus, D. M., and J. Shukla, 2002: Does ENSO force the PNA? *J. Climate*, **15**, 2340–2358.

Takacs, L., M. J. Suarez, and R. Todling, 2016: Maintaining Atmospheric Mass and Water Balance within Reanalysis. Q. J. Royal Meteor. Soc., 142, 1565–1573,doi: 10.1002/qj.2763.

Taylor, K. E., D. Williamson, and F. Zwiers, 2000: The sea surface temperature and sea ice concentration boundary conditions for AMIP II simulations. Program for Climate Model Diagnosis and Intercomparison (PCMDI).Report 60, Lawrence Livermore NationalLaboratory.

Ting, M. F., and H. Wang, 1997: Summertime US precipitation variability and its relation to Pacific sea surface temperature. J. Climate, 10, 1853-1873.

Wallace, J.M. and D.S. Gutzler, 1981: Teleconnections in the Geopotential Height Field during the Northern Hemisphere Winter. Mon. Wea. Rev., 109, 784–812, doi: 10.1175/1520-0493(1981)109<0784:TITGHF>2.0.CO;2.

Westby, R., Y. Lee, and R. Black, 2013: Anomalous Temperature Regimes during the Cool Season: Long-Term Trends, Low-Frequency Mode Modulation, and Representation in CMIP5 Simulations. J. Climate, 26, 9061–9076, doi: 10.1175/JCLI-D-13-00003.1.

Wise, E., M. Wrzesien, M. Dannenberg, and D. McGinnis, 2015: Cool-Season Precipitation Patterns Associated with Teleconnection Interactions in the United States. J. Appl. Meteor. Climatol., 54, 494–505, doi: 10.1175/JAMC-D-14-0040.1.

Wolter, K., R.M. Dole, and C.A. Smith, 1999: Short-Term Climate Extremes over the Continental United States and ENSO. Part I: Seasonal Temperatures. J. Climate, 12, 3255\u20133272, doi: 10.1175/1520-0442(1999)012<3255:STCEOT>2.0.CO;2.

Yoon, J.-H., and L. R. Leung, 2015: Assessing the relative influence of surface soil moisture and ENSO SST on precipitation predictability over the contiguous United States. Geophys. Res. Lett., 42, 5005–5013. doi: 10.1002/2015GL064139.

Zhang, Y., J.M. Wallace, D.S. Battisti, 1997: ENSO-like interdecadal variability: 1900-93. J. Climate, 10, 1004-1020.

Zhang, X., J. Wang, F. Zwiers, and P. Groisman, 2010: The Influence of Large-Scale Climate Variability on Winter Maximum Daily Precipitation over North America. J. Climate, 23, 2902–2915, doi: 10.1175/2010JCLI3249.1.

Zhang, T., M. Hoerling, J. Perlwitz, D. Sun, and D. Murray, 2011: Physics of U.S. Surface Temperature Response to ENSO. J. Climate, 24, 4874–4887, doi: 10.1175/2011JCLI3944.1.

Zhang, T., M. Hoerling, J. Perlwitz, and T. Xu, 2016: Forced Atmospheric Teleconnections during 1979–2014. J. Climate, 29, 2333–2357, doi: 10.1175/JCLI-D-15-0226.1.

6. Web Resources

Supplemental Online Library: https://gmao.gsfc.nasa.gov/multi-partner/NCA/pubs/TM47_suppl/

Appendix A: Fraction of Area with Significant Correlations

	PRCPTOT				R99P				R99D			
	M2AMIP		Obs		M2AMIP		Obs		M2AMIP		Obs	
	-	+	-	+	-	+	-	+	-	+	-	+
DJF Niño3.4	20	24	2	14	5	15	2	8	4	15	3	9
MAM Niño3.4	1	24	0	3	0	3	0	0	0	7	1	6
JJA Niño3.4	5	6	0	1	4	1	0	0	4	1	0	1
SON Niño 3.4	3	14	0	0	1	2	0	1	1	3	0	0
DJF PDO	14	14	1	2	1	4	2	1	2	4	1	0
MAM PDO	1	16	0	1	0	3	2	0	1	3	0	7
JJA PDO	1	8	0	3	1	1	1	2	1	1	0	5
SON PDO	1	8	0	0	1	1	0	0	1	2	0	5
DJF NAO	9	7	1	0	3	2	0	0	4	2	1	0
DJF PNA	38	13	12	1	14	13	7	1	14	13	4	0
MAM PNA	20	14	2	2	5	5	0	2	6	6	4	3
JJA PNA	1	13	0	1	2	2	0	1	2	3	1	1
SON PNA	32	3	2	0	9	0	1	0	11	1	1	0

Table 1: The fraction of land area, as a percentage of total land grid cells in the domain, where the correlation between the teleconnection index and daily precipitation index exceeds the 99th percentile.

	T2M				TN10P				TX90P			
	M2AMIP		Obs		M2AMIP		Obs		M2AMIP		Obs	
	-	+	-	+	-	+	-	+	-	+	-	+
DJF Niño3.4	31	20	0	14	23	23	12	4	33	14	14	7
MAM Niño3.4	24	7	0	1	18	24	5	6	32	15	9	6
JJA Niño3.4	31	3	2	1	4	30	6	8	42	4	13	3
SON Niño 3.4	4	3	0	0	2	47	4	7	40	9	10	2
DJF PDO	35	11	11	6	9	26	10	9	38	8	16	6
MAM PDO	23	3	1	6	9	30	11	7	38	5	10	6
JJA PDO	58	1	6	15	1	57	6	9	59	2	9	5
SON PDO	5	2	1	3	1	53	4	11	48	4	19	3
DJF NAO	9	32	0	29	16	14	10	5	5	39	2	26
DJF PNA	30	28	11	18	32	24	19	4	34	24	16	9
MAM PNA	26	14	1	1	19	32	12	7	35	17	18	3
JJA PNA	52	1	2	1	1	58	5	9	53	5	5	8
SON PNA	0	0	0	0	0	26	4	7	41	0	6	3

Table 2: The fraction of land area, as a percentage of total land grid cells in the domain, where the correlation between the teleconnection index and daily temperature index exceeds the 99th percentile.

Previous Volumes in This Series

Volume 1 *September 1994*	Documentation of the Goddard Earth Observing System (GEOS) general circulation model - Version 1 **L.L. Takacs, A. Molod, and T. Wang**
Volume 2 *October 1994*	Direct solution of the implicit formulation of fourth order horizontal diffusion for gridpoint models on the sphere **Y. Li, S. Moorthi, and J.R. Bates**
Volume 3 *December 1994*	An efficient thermal infrared radiation parameterization for use in general circulation models **M.-D. Chou and M.J. Suarez**
Volume 4 *January 1995*	Documentation of the Goddard Earth Observing System (GEOS) Data Assimilation System - Version 1 **James Pfaendtner, Stephen Bloom, David Lamich, Michael Seablom, Meta Sienkiewicz, James Stobie, and Arlindo da Silva**
Volume 5 *April 1995*	Documentation of the Aries-GEOS dynamical core: Version 2 **Max J. Suarez and Lawrence L. Takacs**
Volume 6 *April 1995*	A Multiyear Assimilation with the GEOS-1 System: Overview and Results **Siegfried Schubert, Chung-Kyu Park, Chung-Yu Wu, Wayne Higgins, Yelena Kondratyeva, Andrea Molod, Lawrence Takacs, Michael Seablom, and Richard Rood**

Volume 7 *September 1995*	Proceedings of the Workshop on the GEOS-1 Five-Year Assimilation **Siegfried D. Schubert and Richard B. Rood**
Volume 8 *March 1996*	Documentation of the Tangent Linear Model and Its Adjoint of the Adiabatic Version of the NASA GEOS-1 C-Grid GCM: Version 5.2 **Weiyu Yang and I. Michael Navon**
Volume 9 *March 1996*	Energy and Water Balance Calculations in the Mosaic LSM **Randal D. Koster and Max J. Suarez**
Volume 10 *April 1996*	Dynamical Aspects of Climate Simulations Using the GEOS General Circulation Model **Lawrence L. Takacs and Max J. Suarez**
Volume 11 *May 1997*	Documentation of the Tangent Linear and Adjoint Models of the Relaxed Arakawa-Schubert Moisture Parameterization Package of the NASA GEOS-1 GCM (Version 5.2) **Weiyu Yang, I. Michael Navon, and Ricardo Todling**
Volume 12 *August 1997*	Comparison of Satellite Global Rainfall Algorithms **Alfred T.C. Chang and Long S. Chiu**
Volume 13 *December 1997*	Interannual Variability and Potential Predictability in Reanalysis Products **Wie Ming and Siegfried D. Schubert**

Volume 14	A Comparison of GEOS Assimilated Data with FIFE Observations
August 1998	**Michael G. Bosilovich and Siegfried D. Schubert**
Volume 15	A Solar Radiation Parameterization for Atmospheric Studies
June 1999	**Ming-Dah Chou and Max J. Suarez**
Volume 16	Filtering Techniques on a Stretched Grid General Circulation Model
November 1999	**Lawrence Takacs, William Sawyer, Max J. Suarez, and Michael S. Fox-Rabinowitz**
Volume 17 *July 2000*	Atlas of Seasonal Means Simulated by the NSIPP-1 Atmospheric GCM **Julio T. Bacmeister, Philip J. Pegion, Siegfried D. Schubert, and Max J. Suarez**
Volume 18 *December 2000*	An Assessment of the Predictability of Northern Winter Seasonal Means with the NSIPP1 AGCM **Philip J. Pegion, Siegfried D. Schubert, and Max J. Suarez**
Volume 19 *July 2001*	A Thermal Infrared Radiation Parameterization for Atmospheric Studies **Ming-Dah Chou, Max J. Suarez, Xin-Zhong Liang, and Michael M.-H. Yan**
Volume 20	The Climate of the FVCCM-3 Model
August 2001	**Yehui Chang, Siegfried D. Schubert, Shian-Jiann Lin, Sharon Nebuda, and Bo-Wen Shen**

Volume 21

September 2001

Design and Implementation of a Parallel Multivariate Ensemble Kalman Filter for the Poseidon Ocean General Circulation Model

Christian L. Keppenne and Michele M. Rienecker

Volume 22

August 2002

A Coupled Ocean-Atmosphere Radiative Model for Global Ocean Biogeochemical Models

Watson W. Gregg

Volume 23

November 2002

Prospects for Improved Forecasts of Weather and Short-term Climate Variability on Subseasonal (2-Week to 2-Month) Time Scales

Siegfried D. Schubert, Randall Dole, Huang van den Dool, Max J. Suarez, and Duane Waliser

Volume 24

July 2003

Temperature Data Assimilation with Salinity Corrections: Validation for the NSIPP Ocean Data Assimilation System in the Tropical Pacific Ocean, 1993–1998

Alberto Troccoli, Michele M. Rienecker, Christian L. Keppenne, and Gregory C. Johnson

Volume 25

December 2003

Modeling, Simulation, and Forecasting of Subseasonal Variability

Duane Waliser, Siegfried D. Schubert, Arun Kumar, Klaus Weickmann, and Randall Dole

Volume 26

April 2005

Documentation and Validation of the Goddard Earth Observing System (GEOS) Data Assimilation System – Version 4

Senior Authors: S. Bloom, A. da Silva and D. Dee

Contributing Authors: M. Bosilovich, J-D. Chern, S. Pawson, S.

Schubert, M. Sienkiewicz, I. Stajner, W-W. Tan, and M-L. Wu

Volume 27

December 2008

The GEOS-5 Data Assimilation System - Documentation of Versions 5.0.1, 5.1.0, and 5.2.0.

M.M. Rienecker, M.J. Suarez, R. Todling, J. Bacmeister, L. Takacs, H.-C. Liu, W. Gu, M. Sienkiewicz, R.D. Koster, R. Gelaro, I. Stajner, and J.E. Nielsen

Volume 28

April 2012

The GEOS-5 Atmospheric General Circulation Model: Mean Climate and Development from MERRA to Fortuna

Andrea Molod, Lawrence Takacs, Max Suarez, Julio Bacmeister, In-Sun Song, and Andrew Eichmann

Volume 29

June 2012

Atmospheric Reanalyses – Recent Progress and Prospects for the Future.

A Report from a Technical Workshop, April 2010

Michele M. Rienecker, Dick Dee, Jack Woollen, Gilbert P. Compo, Kazutoshi Onogi, Ron Gelaro, Michael G. Bosilovich, Arlindo da Silva, Steven Pawson, Siegfried Schubert, Max Suarez, Dale Barker, Hirotaka Kamahori, Robert Kistler, and Suranjana Saha

Volume 30

December 2012

The GEOS-iODAS: Description and Evaluation

Guillaume Vernieres, Michele M. Rienecker, Robin Kovach and Christian L. Keppenne

Volume 31

March 2013

Global Surface Ocean Carbon Estimates in a Model Forced by MERRA

	Watson W. Gregg, Nancy W. Casey and Cecile S. Rousseaux
Volume 32 *March 2014*	Estimates of AOD Trends (2002-2012) over the World's Major Cities based on the MERRA Aerosol Reanalysis **Simon Provencal, Pavel Kishcha, Emily Elhacham, Arlindo M. da Silva, and Pinhas Alpert**
Volume 33 *August 2014*	The Effects of Chlorophyll Assimilation on Carbon Fluxes in a Global Biogeochemical Model **Cécile S. Rousseaux and Watson W. Gregg**
Volume 34 *September 2014*	Background Error Covariance Estimation using Information from a Single Model Trajectory with Application to Ocean Data Assimilation into the GEOS-5 Coupled Model **Christian L. Keppenne, Michele M. Rienecker, Robin M. Kovach, and Guillaume Vernieres**
Volume 35 *December 2014*	Observation-Corrected Precipitation Estimates in GEOS-5 **Rolf H. Reichle and Qing Liu**
Volume 36 *March 2015*	Evaluation of the 7-km GEOS-5 Nature Run **Ronald Gelaro, William M. Putman, Steven Pawson, Clara Draper, Andrea Molod, Peter M. Norris, Lesley Ott, Nikki Prive, Oreste Reale, Deepthi Achuthavarier, Michael Bosilovich, Virginie Buchard, Winston Chao, Lawrence Coy, Richard Cullather, Arlindo da Silva, Anton Darmenov, Ronald M. Errico, Marangelly Fuentes, Min-Jeong Kim, Randal Koster, Will McCarty, Jyothi Nattala, Gary Partyka, Siegfried Schubert, Guillaume Vernieres, Yuri Vikhliaev, and Krzysztof Wargan**

Volume 37

March 2015

Maintaining Atmospheric Mass and Water Balance within Reanalysis

Lawrence L. Takacs, Max Suarez, and Ricardo Todling

Volume 38

September 2015

The Quick Fire Emissions Dataset (QFED) – Documentation of versions 2.1, 2.2 and 2.4

Anton S. Darmenov and Arlindo da Silva

Volume 39

September 2015

Land Boundary Conditions for the Goddard Earth Observing System Model Version 5 (GEOS-5) Climate Modeling System - Recent Updates and Data File Descriptions

Sarith Mahanama, Randal Koster, Gregory Walker, Lawrence Takacs, **Rolf**

Reichle, Gabrielle De Lannoy, Qing Liu, Bin Zhao, and Max **Suarez**

Volume 40

October 2015

Soil Moisture Active Passive (SMAP) Project Assessment Report for the Beta-Release L4_SM Data Product

Rolf H. Reichle, Gabrielle J. M. De Lannoy, Qing Liu, Andreas Colliander,

Austin Conaty, Thomas Jackson, John Kimball, and Randal D. Koster

Volume 41

October 2015

GDIS Workshop Report

Siegfried Schubert, Will Pozzi, Kingtse Mo, Eric Wood, Kerstin Stahl, Mike Hayes, Juergen Vogt, Sonia Seneviratne, Ron Stewart, Roger Pulwarty, and Robert Stefanski

Volume 42

Soil Moisture Active Passive (SMAP) Project Calibration and Validation for the L4_C Beta-Release Data Product

November 2015 **John Kimball, Lucas Jones, Joseph Glassy, E. Natasha Stavros, Nima Madani, Rolf Reichle, Thomas Jackson, and Andreas Colliander**

Volume 43 MERRA-2: Initial Evaluation of the Climate

September 2015 **Michael G. Bosilovich, Santha Akella, Lawrence Coy, Richard Cullather, Clara Draper, Ronald Gelaro, Robin Kovach, Qing Liu, Andrea Molod, Peter Norris, Krzysztof Wargan, Winston Chao, Rolf Reichle, Lawrence Takacs, Yury Vikhliaev, Steve Bloom, Allison Collow, Stacey Firth, Gordon Labow, Gary Partyka, Steven Pawson, Oreste Reale, Siegfried Schubert, and Max Suarez**

Volume 44 Estimation of the Ocean Skin Temperature using the NASA GEOS Atmospheric Data Assimilation System

February 2016

Santha Akella, Ricardo Todling, Max Suarez

Volume 45 The MERRA-2 Aerosol Assimilation

October 2016 **C. A. Randles, A. M. da Silva, V. Buchard, A. Darmenov, P. R. Colarco, V. Aquila, H. Bian, E. P. Nowottnick, X. Pan, A. Smirnov, H. Yu, and R. Govindaraju**

Volume 46 The MERRA-2 Input Observations: Summary and Assessment

October 2016 **Will McCarty, Lawrence Coy, Ronald Gelaro, Albert Huang, Dagmar Merkova, Edmond B. Smith, Meta Sienkiewicz, and Krzysztof Wargan**